JOURNAL OF PETROLOGY | VOLUME 41 | NUMBER 8 | PAGES 1207–1239 | 2000

Petrogenesis and $^{40}Ar/^{39}Ar$ Geochronology of the Brandberg Complex, Namibia: Evidence for a Major Mantle Contribution in Metaluminous and Peralkaline Granites

A. K. SCHMITT[1]*, R. EMMERMANN[2], R. B. TRUMBULL[1], B. BÜHN[2] AND F. HENJES-KUNST[3]

[1]GEOFORSCHUNGSZENTRUM POTSDAM, TELEGRAFENBERG B124, 14473 POTSDAM, GERMANY

[2]INSTITUT FÜR GEOWISSENSCHAFTEN UND LITHOSPHÄRENFORSCHUNG, UNIVERSITÄT GIESSEN, 35390 GIESSEN, GERMANY

[3]BUNDESANSTALT FÜR GEOWISSENSCHAFTEN UND ROHSTOFFE, 30655 HANNOVER, GERMANY

RECEIVED JANUARY 4, 1999; REVISED TYPESCRIPT ACCEPTED DECEMBER 14, 1999

Anorogenic granites of the Brandberg igneous complex in NW Namibia formed during early Cretaceous rifting and continental break-up of Gondwana. A metaluminous series [SiO_2 = 62–77 wt %, molar (Na + K)/Al = 0·8–0·95] includes an early monzonite body, major biotite–hornblende granite, late biotite granite segregations and peripheral dykes of trachydacite. Volumetrically minor peralkaline granites of the Amis complex [SiO_2 = 72–77 wt %, (Na + K)/Al = 1·0–1·5] intrude the main granite and adjacent country rocks. Compared with the metaluminous main granite, these are in part highly enriched in Zr, Nb, Y, U and Th. Initial Nd and Sr isotope ratios of the metaluminous suite are $\varepsilon Nd_{(130\,Ma)}$ from −0·4 to −5·1 and $^{87}Sr/^{86}Sr_{(130\,Ma)}$ from 0·707 to 0·713. The Nd isotopic composition of the peralkaline granites is within this range [$\varepsilon Nd_{(130\,Ma)}$ from −0·7 to −1·9]. ^{40}Ar–^{39}Ar age determinations (132–130 Ma) indicate that the metaluminous and peralkaline units are indistinguishable in age and that they formed contemporaneously with flood basalts and associated felsic volcanism in the Etendeka–Paraná province. The metaluminous suite is modelled as a crustally contaminated (10–40%) fractionate of a tholeiitic basaltic magma (LTZ.H type), and a common basaltic parent is inferred for the metaluminous and peralkaline rocks of the Brandberg complex. Fractional crystallization of plagioclase, clinopyroxene and Fe–Ti oxides of a parental monzonitic magma accounts for major and trace element variations within the metaluminous group, but radiogenic isotope data require addition of 20 and 40% crustal material. Metaluminous leucogranitic dykes and peralkaline granites formed from highly evolved melts (Eu/Eu <0·1) and melt inclusion analysis from arfvedsonite pegmatite indicate that enhanced solubilities in an F-rich peralkaline residual melt could account for observed enrichments of high-field strength elements. Compositional variations within the peralkaline group reflect at least in part late-magmatic mineral segregation and hydrothermal overgrowth.*

KEY WORDS: *anorogenic granite; Etendeka–Paraná volcanism; Ar–Ar dating; metaluminous–peralkaline suites; AFC processes*

INTRODUCTION

The genesis of anorogenic granitoids remains controversial, especially because of the diversity of rocks grouped under that category, commonly termed 'A-type' (see Eby, 1990, 1992). The range of petrogenetic models suggested for anorogenic granite suites includes crustal anatexis, of either igneous tonalitic–granitic compositions or metasedimentary sources depleted by a prior melting event (Collins *et al.*, 1982; Clemens *et al.*, 1986; Whalen *et al.*, 1987; Creaser *et al.*, 1991; Skjerlie & Johnston, 1993; Patiño Douce, 1997), or fractionation of parental

*Corresponding author. Telephone: +49(0)331-288-1468. Fax: +49(0)331-288-1474. e-mail: axelk@gfz-potsdam.de

Extended data set can be found at: http://www.petrology.oupjournals.org

basaltic magmas with or without assimilation of crustal material (Tronnes & Brandon, 1992; Turner *et al.*, 1992). From previous studies, it is clear that the 'A-type' group of granitoids encompasses very different tectonic settings and modes of origin, especially when both metaluminous and peralkaline occurrences are considered (King *et al.*, 1997).

The Mesozoic igneous complexes in northern and central Namibia occur in a well-exposed and geologically well-investigated extensional tectonic setting. After nearly 400 My of relative quiescence following the late Precambrian Damara Orogeny [see review by Miller (1983)] the area experienced tectonic and magmatic activity associated with the early Cretaceous break-up of western Gondwanaland and the activity of the Tristan mantle plume (Milner & le Roex, 1996). A number of anorogenic granites formed at this time, among which the most prominent are the Brandberg and Erongo complexes. These high-level intrusions are part of an extensive Cretaceous igneous province in Namibia and the Atlantic margin of South America, which includes voluminous continental flood basalts and associated silicic volcanics of the Etendeka–Paraná province (Erlank *et al.*, 1984; Peate *et al.*, 1992, 1999; Garland *et al.*, 1995; Milner & le Roex, 1996; Peate & Hawkesworth, 1996; Peate, 1997) and a variety of Si-saturated and -undersaturated subvolcanic complexes. Many previous studies of the Cretaceous magmatism in Namibia focused on flood basalts and on the mafic members of the subvolcanic complexes (e.g. Okenyenya, Milner & le Roex, 1996; Messum, Ewart *et al.*, 1998*a*). Several studies have addressed the petrogenesis of the silicic volcanics (Milner, 1988; Garland *et al.*, 1995; Harris & Milner, 1997; Ewart *et al.*, 1998*b*; le Roex & Lanyon, 1998). The felsic intrusive complexes, however, have received less attention.

The Brandberg complex is among the largest of the Cretaceous anorogenic granites in Namibia. It shares many structural and compositional features with other anorogenic granite complexes world wide: rift-related setting, high emplacement level, a circular intrusive pattern and associated ring-dykes, an inferred high magmatic temperature, relative paucity of hydrous mineral phases, high Fe/Mg ratios of bulk rock and minerals, low Ca and Sr, high Ga/Al, high contents of high field strength elements (HFSE) (e.g. Zr, Y, Nb), and metaluminous to peralkaline compositions.

Our study of the Brandberg complex has two main objectives: one is to investigate the origin of the main metaluminous granite in the context of the Cretaceous Etendeka–Paraná igneous activity; the other is to investigate the age and genetic relationships between the main granite and a satellite peralkaline granite, the Amis intrusion. The second point is of particular interest in light of the debated role of fluid metasomatism for the genesis of peralkaline granites and the origin of extreme trace element enrichments in these type of granites as emphasized by Bowden *et al.* (1990) and Diehl (1990).

We present for the first time $^{40}Ar/^{39}Ar$ ages and Sr and Nd isotopic data covering the metaluminous and peralkaline rocks of the Brandberg complex, estimates of magmatic temperatures from mineral equilibria and quantified geochemical models of magma evolution.

GEOLOGY

The Brandberg is one of a group of about 20 early Cretaceous igneous complexes which occur along a NE–SW trending zone extending ~350 km inland from the coast at Cape Cross (Fig. 1). They were emplaced into late Precambrian to Cambrian metasedimentary sequences and granites of the Damara Orogen (Porada, 1979, 1989; Miller, 1983). The main focus of Cretaceous magmatism was at the site of the present coastline, where extensive flood basalt and silicic volcanism of the Etendeka Group (Namibia) and the coeval Paraná Province (Brazil) formed at ~132 ± 1 Ma (Renne *et al.*, 1992, 1996; Milner *et al.*, 1995*b*; Stewart *et al.*, 1996). Marine seismic reflection surveys reveal the presence of seaward-dipping reflector sequences on both sides of the South Atlantic, which are interpreted as submerged flood basalt sheets on the continental shelf (Gladczenko *et al.*, 1997). The oldest linear magnetic anomaly on the oceanic crust off Namibia, which marks the onset of sea-floor spreading, is correlated with M4 (~130 Ma; Rabinowitz & LaBrecque, 1979). It is generally believed that the break-up-related volcanism and intrusive activity on the conjugate margins of Namibia and Brazil were caused by the Tristan mantle plume (O'Connor & le Roex, 1992; Milner & le Roex, 1996; Ewart *et al.*, 1998*a*).

The Brandberg complex comprises a nearly circular body of granite in plan view, ~23 km in diameter, which forms a prominent mountain looming some 2000 m above the peneplain of the Damaraland basement. Associated felsic dykes occur at the northeastern edge and subparallel to the rim of the main intrusion and dip ~30–40° towards the centre. Around the base of the Brandberg granite massif is a ring of low hills formed by Damaran granites and metasediments covered by Mesozoic sedimentary and volcanic rocks of the Karoo and Etendeka Groups. The sedimentary sequence is overlain by flood basalts capped by felsic lavas, which are similar to the quartz latites of the Awahab Formation exposed in the Goboboseb mountains southwest of the Brandberg. The Mesozoic cover rocks are preserved in a collar along the western and southern margin of the massif and are tilted towards the contact at 10–20°. Granite apophyses locally intrude as sills into the inclined sequence. At the contact zone the Karoo and Etendeka rocks are downfaulted towards the centre of the massif,

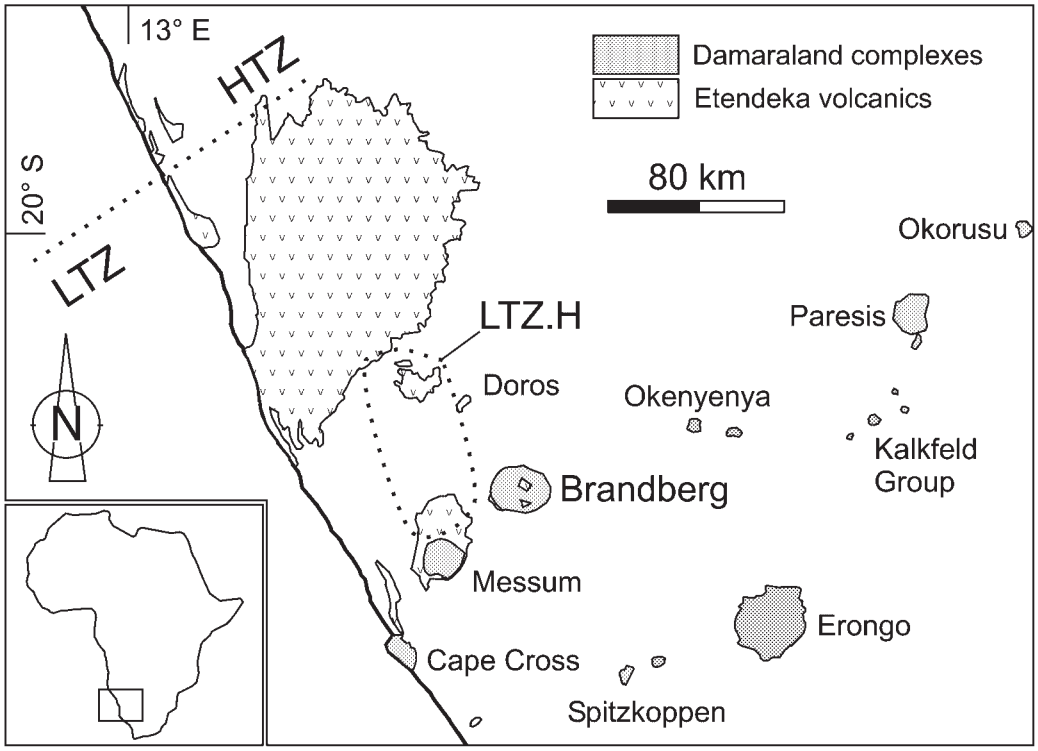

Fig. 1. Simplified geological map of north–central Namibia showing the distribution of Cretaceous igneous complexes and Etendeka group volcanic rocks. The dotted line is the approximate outcrop limit of high-Ti and -Zr (HTZ) basalts in the northern and low-Ti and -Zr (LTZ) basalts in the southern region (Milner & le Roex, 1996). The approximate outcrop of LTZ.H basalts as described by Ewart *et al.* (1998*a*) is also outlined.

producing dips of 60° to near-vertical. Rotated country rock fragments, veined and cemented by a granitic matrix, form a contact breccia in this area. Thermal overprint of the Karoo sediments along the margin of the massif produced an inward dipping contact metamorphic aureole of andalusite-bearing hornfels. These observations led Korn & Martin (1954) to propose a near-surface emplacement in a caldera sag-structure, initiated by minor eruptive magma withdrawal and magma ascent compensated by subsidence of a roof-block. The products of the volcanic activity are no longer preserved outside the complex except, perhaps in part, as roof pendants of quartz–feldspar porphyries (dacitic to rhyolitic in composition) found in the upper reaches of the Brandberg massif.

Early investigations (Cloos & Chuboda, 1931; Hodgson, 1972, 1973) were extended by Diehl (1990), who published the first geochemical study of the Brandberg and presented a new map of the complex, which subdivides the granite massif into a number of concentrically arranged units interpreted as ring dykes. Our study has not confirmed this subdivision and we consider the Brandberg complex to consist of four essentially discrete and mappable intrusive units (Fig. 2): the main hornblende–biotite granite massif, an early quartz monzonite body, the Amis peralkaline granite and peripheral felsic dykes.

FIELD AND PETROGRAPHIC CHARACTERISTICS

Granites of the main massif

The main granite massif consists predominantly of coarse-grained, equigranular hornblende–biotite granite. Diehl (1990) showed a continuous ring of 'hornblende–pyroxene granite' up to 3 km wide along the perimeter of the massif and a discontinuous ring of 'fayalite–hedenbergite' granite at the western and eastern margins. Our sampling along two profiles at the southern and western margins of the massif (Amis and Numas valleys), however, suggests that the unit described as 'hornblende–pyroxene' granite is in fact a biotite–hornblende granite with local cores of clinopyroxene surrounded by hornblende. Fayalite relicts were not found in any samples. Minor variations in texture and in the proportion of mafic minerals are characteristic of the main massif, but as will be shown below, the chemical composition is rather uniform.

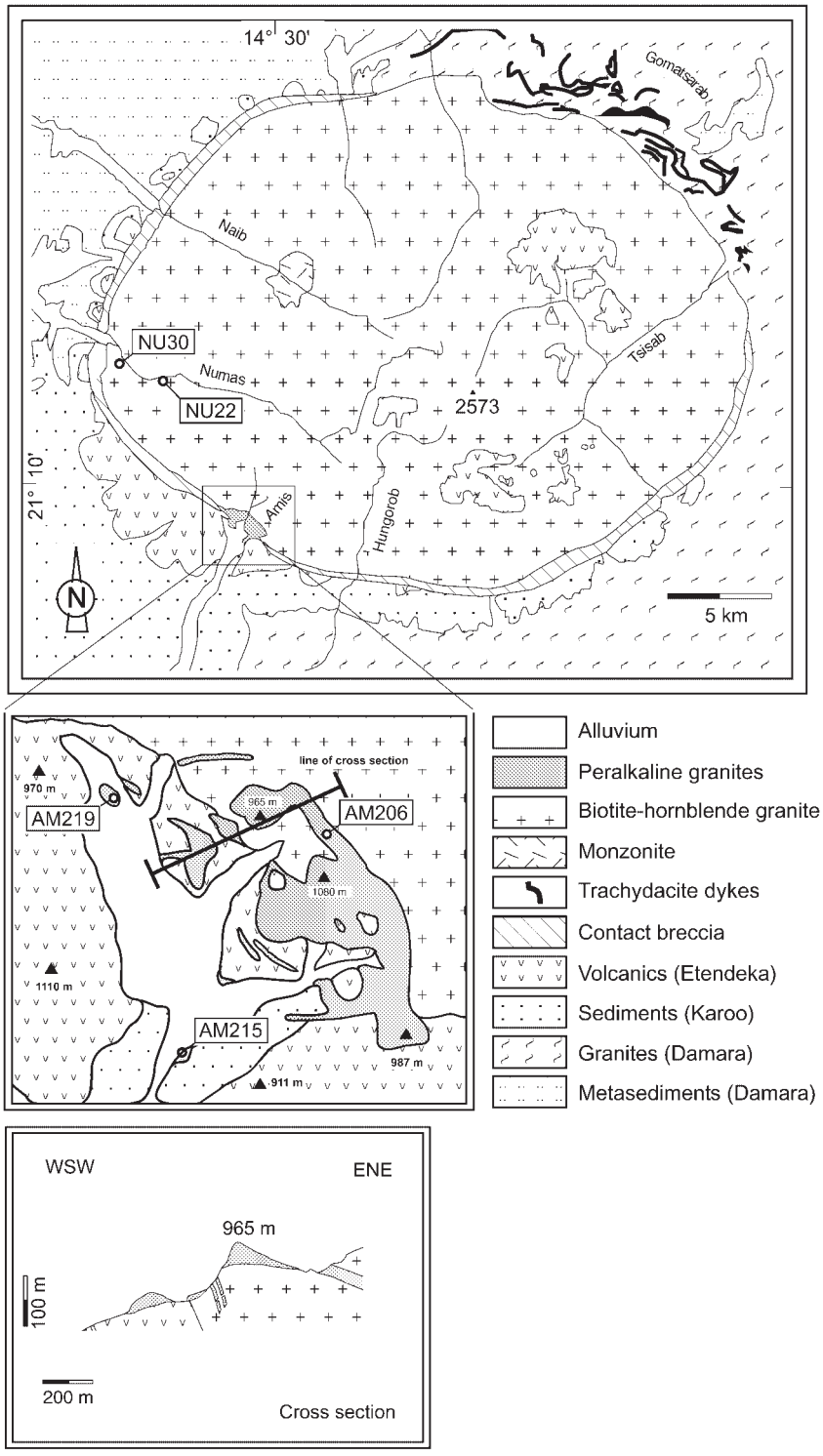

Fig. 2. Geological map of the Brandberg and the Amis complex at the SW edge of the Brandberg including a schematic profile of the Amis intrusion [Amis complex mapped by authors; Brandberg map modified after Hodgson (1972)]. Sample locations for age determinations are indicated on maps.

The hornblende–biotite granite has a hypidiomorphic, medium-grained, equigranular texture. Main minerals include 36–38 wt % of normally zoned plagioclase with maximum An_{33} in cores, which is characteristically rimmed by perthitic orthoclase (23–28 wt %; see Fig. 3a and Table 1). The modal abundance of quartz is between 19 and 24 wt %. Granophyric intergrowths of orthoclase and quartz are common and albite occurs as a fine-grained interstitial phase. Mafic minerals make up a total of ~10–15 wt % and include edenitic hornblende, which commonly contains relict cores of augite ($En_{15}Fs_{46}Wo_{39}$, Fig. 3b), and biotite (*mg*-number = 15–20; see Tables 2 and 3 and Fig. 4). Opaque minerals are exsolved Ti-rich magnetite and ilmenite. Accessories include apatite and zircon, allanite, titanite, chevkinite and thorite. Ferroactinolitic hornblende, chlorite, epidote, sericite and haematite occur as secondary minerals.

Dykes and schlieren of leucocratic granite, some with pegmatitic or aplitic texture, are abundant in the central part of the Brandberg main massif. The dykes show no preferred orientation and range in width from a few tens of centimetres to ~3 m. The main minerals in these rocks are alkali feldspar (perthite), quartz (35 wt %) and nearly pure interstitial albite. A granophyric texture is present in some samples. The main mafic mineral (<5 wt %) is a low-Ti, low-Mg biotite (*mg*-number = 3–10; see also Table 3). Tourmaline occurs locally and accessory minerals include fluorite and zircon.

Monzonite

A volumetrically minor but petrogenetically important igneous unit in the Brandberg complex is a body of coarse-grained monzonite, ~2 km in diameter, exposed in the Naib gorge in the western interior of the massif at an elevation of ~1300 m, i.e. some 1000 m below the top of the massif and 700 m above its base (Fig. 2). Contact relations suggest that the monzonite is older than the Brandberg hornblende–biotite granite because the granite develops a finer-grained porphyritic margin at the monzonite contact, and the monzonite is locally cut by apophyses of the granite. Diehl (1990) cited field evidence for a younger age of the monzonite (chilled margin against the Brandberg granite), for which we found no evidence.

The monzonite consists of large normally zoned plagioclase crystals (core An_{40}, rim An_{10}; see Table 1) in a matrix of fine-grained, granophyric quartz and K-feldspar intergrowths. Compared with the hornblende–biotite granite, augite is more abundant (~10 wt %) and more Mg rich ($En_{27}Fs_{36}Wo_{37}$; see Table 2). Amphibole is late magmatic and of ferro-actinolitic composition. Fe-rich biotite (*mg*-number = 16) and exsolved Ti-magnetite and ilmenite occur as minor phases. Accessory minerals include apatite and zircon.

Amis peralkaline intrusion

The Amis intrusion consists of numerous sills and dykes of peralkaline granite, which cut the main Brandberg massif and adjacent country rocks in an area of ~3 km^2 at the SW margin of the Brandberg (Fig. 2). The main sill of the Amis intrusion reaches a maximum thickness of ~50 m. Dykes with only a few decimetres thickness intruded the country rocks along fractures over distances of >30 m, suggesting that the peralkaline magma had a low viscosity. The Amis intrusion is made up of geochemically highly fractionated peralkaline arfvedsonite and aegirine granites, locally extremely enriched in elements of economic importance such as Nb and the rare earth elements (REE). Field relations offer conclusive evidence that the peralkaline nature of the arfvedsonite granite is a magmatic feature and was not imposed by metasomatism. First, the peralkaline granite exhibits a range of different textural varieties including pegmatitic and aplitic bodies as well as the dominant, fine-grained granite, all of which are arfvedsonite bearing. Second, sharp intrusive contacts are observed between the arfvedsonite granites and both the granites of the main massif and the volcanic country rocks. Mapping (Fig. 2) revealed the presence of enclaves of main granite in arfvedsonite granite matrix and apophyses of arfvedsonite granite, which cut the main granite at their contact. The peralkaline granites clearly post-date the granite of the main massif, as also asserted by Diehl (1990) but later contradicted by the K–Ar dating of Amis granites and granites of the main massif by Watkins *et al.* (1994).

The peralkaline granites differ greatly in texture but all share similar mineralogical and chemical characteristics. The peralkaline bulk-rock composition is reflected in the presence of alkali amphibole (arfvedsonite) and minor pyroxene (aegirine) as the dominant mafic phases. The dominant rock type is a medium-grained arfvedsonite-bearing alkali feldspar granite with strong local variations in mafic mineral abundance. Some outcrops show distinct centimetre-scale layering with alternating arfvedsonite abundances of <5 vol. % in leucocratic layers to ~25 vol. % in the melanocratic layers. In particular, the basal layer of the peralkaline granite sill is highly depleted in mafic components with interstitial arfvedsonite, giving the rock a blotchy appearance. Arfvedsonite is commonly rimmed by aegirine. Quartz, microcline and albite are the dominant felsic minerals. The peralkaline granites are rich in accessory phases including REE-bearing fluorite, bastnaesite, pyrochlore, monazite, xenotime and zircon. Dalyite, a rare zirconium silicate ($K_2ZrSi_6O_{15}$), occurs as an interstitial accessory phase, which has been cited as indicative of high peralkalinity in acid rocks [e.g. in plutonic inclusions of Ascension described by Harris (1983); see also Harris & Rickard (1987)]. Compositionally similar to the arfvedsonite granite are dykes

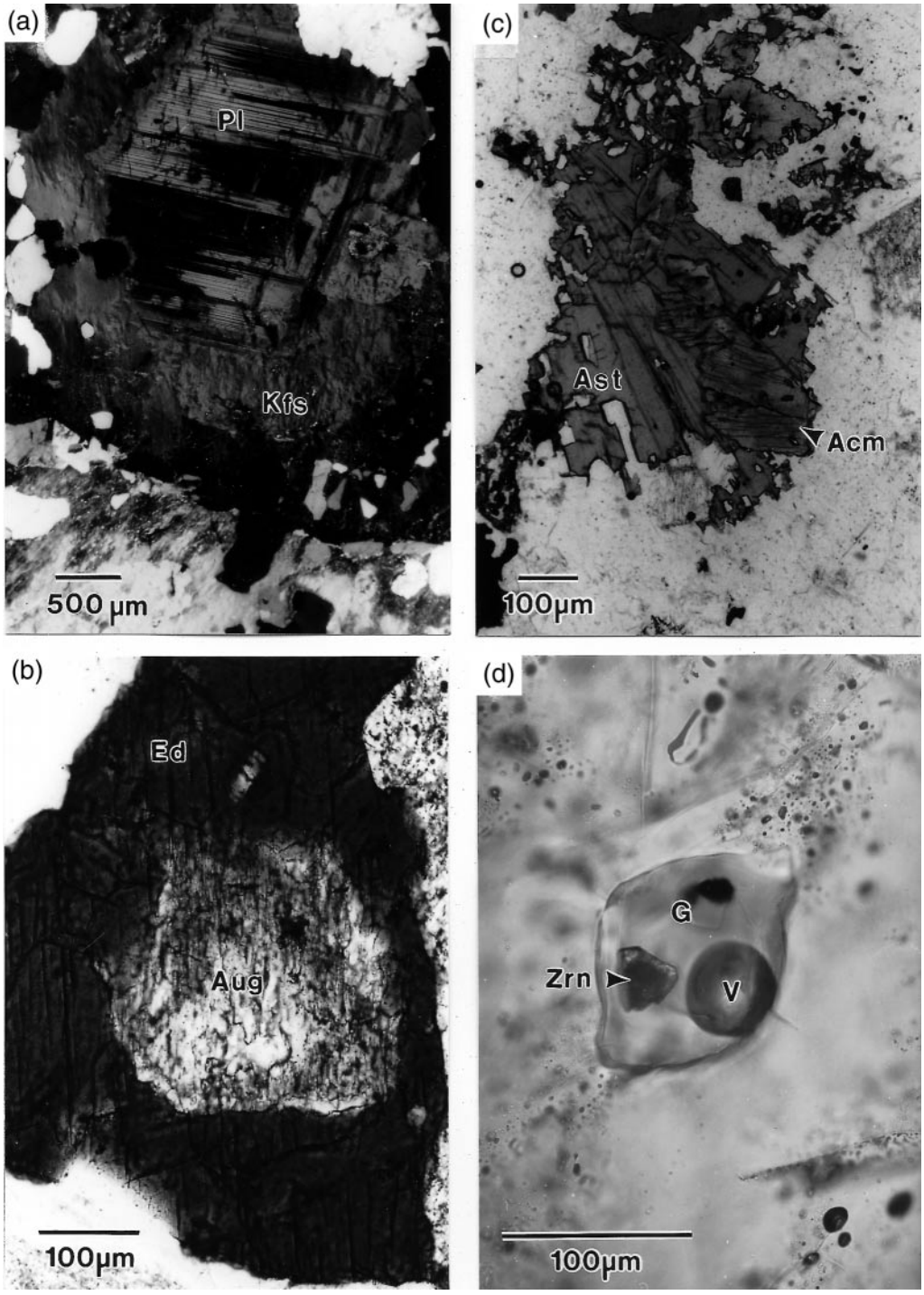

Fig. 3. (a) Microphotograph showing plagioclase (Pl) mantled by microperthitic orthoclase (Kfs) in biotite–hornblende granite NU30 (polars crossed). (b) Augite (Aug) mantled by edenitic hornblende (Ed) in biotite–hornblende granite NU40. (c) Astrophyllite (Ast) and aegirine in quartz–albite matrix from aegirine–albite granite AM219. (d) Glassy melt inclusion (G) from an arfvedsonite-bearing peralkaline pegmatite. Inclusion contains one vapour-filled bubble (V; ~7% of total inclusion volume) and a zircon crystal (Zrn) identified by electron microprobe analysis. Similar zircon crystals commonly occurred in heated inclusions and are due to incomplete homogenization. Zr contents from glass analysis therefore represent minimum values.

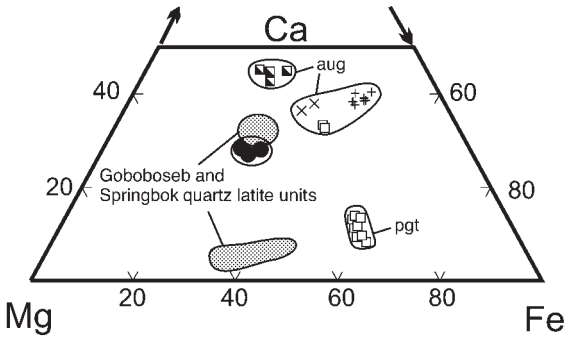

Fig. 4. Pyroxene compositions of Brandberg metaluminous plutonic rocks, trachydacites, internal and peripheral felsic volcanic rocks (aug, augite; pgt, pigeonite; ×, monzonite; +, biotite–hornblende granite; □, trachydacite dykes; ◪, quartz–feldspar porphyry; ●, peripheral felsic lava). Fields show compositional range for pyroxene phenocrysts in Etendeka acidic lavas from the Springbok and Goboboseb quartz latite units [data from Ewart *et al.* (1998*b*)].

that cut the granites of the main massif and volcanic rocks of the peripheral rim. Texturally, these dykes are a fine-grained and saccharoidal variety of peralkaline granite, and were originally termed 'Brandbergite' (Cloos & Chudoba, 1931), a name that was then erroneously used by Hodgson (1973) for leucogranitic aplites occurring in the main massif of the Brandberg.

Some samples of the arfvedsonite granite show clear evidence of post-magmatic recrystallization, such as growth of quartz occasionally replacing feldspars. This is accompanied locally by pervasive haematization. Quartz–haematite intergrowths replace arfvedsonite, which is preserved only where armoured by quartz. This type of replacement produced a reddened and highly indurated variety of granite, which forms prominent cliffs of ~50 m height in the central part of the Amis complex.

A compositionally extreme variety of peralkaline granite occurs as fine-grained mesocratic segregations in the western part of Amis valley. These rocks have a characteristic spotted appearance caused by radiating clusters of aegirine. They contain quartz and albite as the main constituents, ~5 wt % aegirine, and are extremely rich in accessory minerals (astrophyllite, Nb–Zn-rich ilmenite, pyrochlore, thorite and zircon; see Fig. 3c). Zircon is compositionally zoned, with poikilitic and metamict cores overgrown by clear rims, which have a lower Zr/Hf ratio (cores 25, rims 10).

Peripheral dykes

The country rocks at the NNE margin of the complex near Gomatsarab are cut by porphyritic felsic dykes up to 30 m in outcrop width, many of which strike subparallel to the rim of the Brandberg massif. The distribution of the dykes and their proximity to the Brandberg margin, as well as their chemical composition (see below) clearly indicate that they are related to the Brandberg intrusion. However, the relative timing is not known because no intrusive contact between the dykes and the main granite is exposed. Diehl (1990) interpreted the

Table 1: Selected microprobe analyses of feldspars from the Brandberg complex (in wt %)

Sample:	GO10	GO10	B21a	B21a	NU40	NU40	NU40	AM71	AM71	AM207	AM207
Rock unit:	td	td	m	m	mgr	mgr	mgr	mgr	mgr	am	am
Mineral:	pl	pl	pl	pl	pl	pl	kfs	pl	pl	ab	kfs
	core	rim	core	rim	core	rim	rim	core	rim	—	—
SiO_2	57·79	60·00	59·37	63·85	59·82	66·93	64·86	63·81	64·71	68·29	64·12
Al_2O_3	25·43	24·44	25·19	22·68	24·72	20·99	19·30	22·46	19·89	18·77	17·52
Fe_2O_3*	0·43	0·48	0·34	0·06	0·31	0·33	0·10	0·13	0·19	0·94	1·22
CaO	8·33	6·73	6·71	2·50	6·09	1·51	0·57	3·54	1·32	n.d.	n.d.
BaO	0·12	0·16	0·10	n.d.	0·11	0·01	0·31	n.d.	n.d.	n.d.	n.d.
Na_2O	6·08	7·08	7·10	10·39	7·38	9·71	5·06	9·70	4·57	11·28	0·84
K_2O	0·82	0·79	0·65	0·37	0·64	0·34	8·54	0·07	9·27	0·21	15·42
Total	99·00	99·69	99·46	99·85	99·08	99·82	98·74	99·72	99·95	99·49	99·12
Ab	54·2	62·6	63·2	86·5	66·1	90·2	46·0	82·9	40·1	98·8	7·7
Or	4·8	4·6	3·8	2·0	3·8	2·1	51·1	0·4	53·5	1·2	92·4
An	41·0	32·9	33·0	11·5	30·1	7·8	2·9	16·7	6·4	0·0	0·0

Rock units: td, trachydacite; m, monzonite; mgr, main hornblende–biotite granite; am, peralkaline granite. Minerals: pl, plagioclase; kfs, K-feldspar; ab, albite. n.d., not detected.
Fe_2O_3* is total Fe as Fe_2O_3.

Table 2: Selected microprobe analyses of pyroxene from the Brandberg complex (in wt %)

Sample:	GO10	GO10	B21a	B21a	AM64	AM64	B23V	B23VI	AM213	AM218
Rock unit:	td	td	m	m	mgr	mgr	qfp	qfp	am	am
Mineral:	pgt	aug	aug	aug	aug	aug	aug	aug	acm	acm
SiO_2	47·82	48·03	49·91	49·71	48·78	48·41	49·21	50·55	50·70	51·53
TiO_2	0·36	0·56	0·61	0·71	0·40	0·40	0·15	0·11	1·11	1·50
Al_2O_3	0·71	1·22	0·93	1·14	1·05	1·11	0·91	0·90	0·67	0·56
Na_2O	0·12	0·22	0·26	0·27	0·58	0·67	0·41	0·22	12·80	13·21
FeO*	33·02	24·15	21·02	19·93	23·63	24·07	15·67	13·95	29·60	28·53
FeO	29·80	21·07	20·44	19·27	22·58	22·05	12·07	11·32	3·82	3·51
Fe_2O_3	3·58	3·43	0·65	0·74	1·17	2·25	4·00	2·90	28·65	27·81
MnO	0·94	0·75	0·55	0·58	1·15	1·23	1·21	1·01	0·19	0·15
MgO	10·32	8·95	8·55	9·62	5·70	5·69	10·74	10·73	0·06	0·02
CaO	6·55	15·78	17·84	17·09	17·24	17·00	20·82	22·72	0·26	0·04
Total	100·19	100·01	99·74	99·13	98·65	98·81	99·52	100·49	98·27	98·33
Ca	13·8	33·1	38·3	36·8	38·7	38·0	42·5	46·1	—	—
Mg	30·3	26·1	25·5	28·8	17·8	17·7	30·5	30·3	—	—
ΣFe	55·9	40·8	36·2	34·5	43·5	44·2	26·9	23·7	—	—
mg-no.	35·1	39·0	41·4	45·5	29·1	28·6	53·1	56·1	<1·0	<1·0

Rock units: td, trachydacite; m, monzonite; mgr, main hornblende–biotite granite; qfp, quartz–feldspar porphyry; am, peralkaline granite. Minerals: pgt, pigeonite; aug, augite; acm, aegirine. FeO* is total Fe as FeO. Fe^{2+}/Fe^{3+} calculated from charge balance and stoichiometry after Droop (1987); atomic percentages of Ca, Mg, ΣFe calculated according to Deer *et al.* (1992); *mg*-number = 100 × Mg/(Mg + Fe + Mn) molar. n.d., not detected.

dykes as cone sheets intruded before emplacement of the main granite, but Hodgson (1972) described the dykes as representing the final phase of intrusion. As the dyke rocks are isotopically slightly more evolved than the main granite, we prefer to interpret them as coeval or late intrusions formed during emplacement and updoming of the Brandberg magma body.

The dykes are trachydacites according to the IUGS total alkali vs silica classification (LeBas *et al.*, 1986). The dark, fine-grained rocks are porphyritic, with plagioclase phenocrysts up to ~3 mm length. Plagioclase is normally zoned (core An_{40}, rim An_{30}; Table 1). Anhedral Fe-rich pigeonite ($En_{31}Fs_{57}Wo_{12}$, Table 2) is often rimmed by secondary ferro-actinolitic hornblende. Rare individual grains of augite ($En_{26}Fs_{40}Wo_{24}$, Table 2) have also been identified. Other mafic silicates are edenitic hornblende and rare biotite. The matrix consists of microcrystalline granophyric intergrowths of quartz and alkali feldspar. Accessory phases, in order of decreasing abundance, are Ti-rich magnetite ($Mag_{38}Usp_{62}$), apatite and zircon.

The trachydacite dykes resemble the regionally exposed quartz latites of the Awahab Formation in terms of mineralogy, texture and major element composition (Ewart *et al.*, 1998*b*). The compositions of plagioclase phenocrysts overlap, whereas pigeonites of the trachydacite dykes have higher Fe contents compared with those in the Awahab quartz latites (Fig. 4), and the trace element and isotopic characteristics show clear differences (see below).

Quartz–feldspar porphyries from the roof zone of the massif contain phenocrysts of quartz, normally zoned plagioclase (core An_{46}, rim An_{30}) and augite ($En_{30}Fs_{26}Wo_{44}$) in a microcrystalline groundmass. Augite from these quartz–feldspar porphyries is more calcic than augite from the felsic lavas on top of the Karoo sediments and Etendeka basalts at the southwestern margin of the Brandberg. Their augite composition in turn overlaps with clinopyroxene data of quartz latites from the Awahab Formation (Fig. 4). Mineral compositions together with whole-rock trace element abundances (see below) therefore underscore that the peripheral and the roof pendant felsic volcanics of the Brandberg are stratigraphically distinct.

ANALYTICAL METHODS

Electron microprobe analyses were carried out on a Cameca SX 50 electron microprobe fitted with argon flow

Table 3: Selected microprobe analyses of amphibole and biotite from the Brandberg complex (in wt %)

Sample:	GO10	B21a	NU40	NU30	NU22	NU22	AM71	B21a	NU22	B6	AM205[1]
Rock unit:	td	m	mgr	mgr	mgr	mgr	mgr	m	mgr	blg	am
Mineral:	Fe-ed	Fe-act	Fe-ed	Fe-ed	Fe-ed	Fe-ed	Fe-ed	bt	bt	bt	arf
SiO_2	43·33	46·36	41·43	41·05	40·10	40·05	40·16	34·08	34·05	36·76	49·41
TiO_2	0·75	0·17	0·47	1·68	1·41	1·53	1·23	3·48	3·36	1·99	1·06
Al_2O_3	6·30	3·76	7·32	7·57	8·07	7·62	7·61	12·77	11·68	18·02	1·06
FeO*	25·90	31·49	27·69	25·74	27·78	27·51	29·00	33·47	32·41	26·27	32·27
FeO	25·90	29·88	24·88	25·74	27·33	27·51	26·18	—	—	—	—
Fe_2O_3	0·00	1·79	3·13	0·00	0·50	0·00	3·13	—	—	—	—
MnO	0·40	0·68	0·83	0·64	0·85	0·92	1·06	0·31	0·44	n.d.	0·46
MgO	6·45	3·38	4·75	5·25	4·01	3·67	3·53	2·71	3·39	1·14	0·04
CaO	10·06	10·02	10·11	9·79	9·99	10·00	10·34	n.d.	0·06	n.d.	0·38
Na_2O	1·86	0·67	1·86	2·03	2·02	2·42	1·89	0·02	0·11	0·15	8·62
K_2O	1·14	0·35	1·00	1·12	1·14	1·12	1·25	9·51	8·75	9·12	1·42
F	1·03	0·33	0·87	1·51	0·97	0·98	0·58	0·05	0·78	4·28	2·26
Cl	0·30	0·11	0·22	0·20	0·23	0·23	0·19	n.d.	0·43	n.d.	n.d.
–O=F	−0·43	−0·14	−0·37	−0·64	−0·41	−0·41	−0·24	−0·02	−0·33	−1·80	−0·95
–O=Cl	−0·07	−0·02	−0·05	−0·05	−0·05	−0·05	−0·04	0·00	−0·10	0·00	—
Total	97·43	97·41	96·77	96·49	96·53	95·96	96·75	96·38	95·03	95·93	96·80
mg-no.	30·4	16·2	22·9	26·2	20·0	18·7	17·3	12·5	15·5	7·2	<1·0

[1]Contains 0·4 wt % Zn.
Rock units: td, trachydacite; m, monzonite; mgr, main hornblende–biotite granite; blg, biotite leucogranite; am, peralkaline granite. Minerals: Fe-ed, ferro-edenite; Fe-act, ferro-actinolite; bt, biotite; arf, arfvedsonite. FeO* is total Fe as FeO. FeO and Fe_2O_3 are for the minimum ferric Fe estimate calculated from charge balance and stoichiometry for 15 cations excluding $(Na + K)_A$ after Schumacher (1997). *mg*-number = 100 × Mg/(Mg + Fe + Mn) molar. n.d., not detected.

counters. PAP corrections were applied using Cameca software (Pouchou & Pichoir, 1984). The accelerating voltage used was 15 kV for major phases, and constant beam currents of 20 and 10 nA were used, depending on the material analysed. Beam spot size averaged 3 μm for mineral analysis. Natural and synthetic mineral standards were used. For melt inclusion analysis, thick sections (~500 μm) of quartz were heated at 890°C for 20 h at atmospheric pressure and then rapidly quenched using liquid N_2. Melt inclusions were then exposed and polished for electron microprobe analysis. A 15 μm beam diameter was used for glass inclusion analysis to minimize effects of sodium loss. Bulk-rock compositions were analysed using a Philips PW 1400 X-ray fluorescence (XRF) spectrometer with an Rh tube. Fused discs were used for major elements and pressed powder briquettes for Zn, Ga, Rb, Sr, Y, Zr, Nb and Th. FeO was determined by manganometric titration after digestion of rock powder in HF–H_2SO_4. CO_2 was determined coulometrically (Ströhlein Coulomat 701) and H_2O by Karl-Fischer titration (Mitsubishi Moisture Meter). F and Cl were determined using ion-specific electrodes following hydropyrolytic extraction. REE and trace elements (Sc, Zn, Co, Ga, Rb, Sr, Y, Nb, Cs, Ba, Ta, Pb, Th and U in Table 4) were analysed by inductively coupled plasma mass spectrometry (ICP-MS) after digestion in HF–$HClO_4$. Accuracy of ICP-MS determinations was monitored using international geological reference materials (JG-2 and JR-2), and relative deviations between measured and reported values were <10%. For isotopic determinations, whole-rock powders were dissolved in pressurized Teflon vessels for 3 days in 5:1 HF–HNO_3. The Sr and REE fractions were separated in quartz glass columns using cation exchange resin Biorad AG50Wx12. Neodymium was separated from the REE fraction in quartz glass columns filled with Teflon powder (PFTE) coated with HDEHP(bis-2 ethyl-hexyl-phosphoric acid). The Sr isotopic composition was measured with a VG Sector 54-30 mass spectrometer operated in the dynamic mode. Mass fractionation was corrected using the ratio of $^{88}Sr/^{86}Sr = 8{\cdot}3752$. The average value for $^{87}Sr/^{86}Sr$ obtained from NBS 987 during the period of this study was $0{\cdot}710246 \pm 10$ (2σ). The Nd isotope analysis was made on a Finnigan MAT 262 mass spectrometer operated in the static mode and using a double-filament procedure (Ta evaporation filament, Re ionization

filament). Mass fractionation was corrected using the $^{146}Nd/^{144}Nd$ ratio of 0·7219. Repeated analysis of the La Jolla Nd standard yielded a value of $^{143}Nd/^{144}Nd = 0{\cdot}511855 \pm 8$ (2σ). The Sr and Nd initial isotopic ratios were calculated using Rb/Sr and Sm/Nd ratios from chemical analysis.

$^{40}Ar/^{39}Ar$ dating was performed at the Bundesanstalt für Geowissenschaften und Rohstoffe (BGR), Hannover, via incremental heating of mineral separates following the method described by Faryad & Henjes-Kunst (1997). Biotite (biotite–hornblende granite), sodic amphibole (peralkaline granite) and astrophyllite (aegirine–albite granite) were separated from crushed samples by sieving, heavy liquid and magnetic separation, and final hand-picking. Grain sizes ranged between 180 and 355 μm. Sample aliquots of ~50–150 mg, depending on potassium concentrations, were analysed. The gas release behaviour was checked in a pre-run to optimize a step-heating procedure. Gas was extracted during 11–19 heating steps, each step retaining a constant temperature for 30 min, up to a maximum temperature of 1550°C to ensure total degassing of the samples. Measured isotopic ratios were corrected for mass discrimination, total-system blank, decay of ^{39}Ar and ^{37}Ar, and for interfering isotopes. The $^{40}Ar/^{39}Ar$ apparent ages of the samples were normalized to 24·42 Ma for the HD-B1 standard biotite (Hess & Lippolt, 1994). Compatibility of ages with previously published Ar–Ar dates is ensured by comparison of our K–Ar age for the standard glauconite GL-O (94·5 Ma), which corresponds to an apparent age of 520·6 Ma for standard amphibole MM Hb-1 (Odin, 1993). Renne *et al.* (1996) reported their Ar–Ar ages relative to MM Hb-1 = 520·4 Ma.

The error in the $^{40}Ar/^{39}Ar$ step ages was calculated by error propagation of uncertainties including those of the in-run statistical parameters and the errors derived from the blank contributions, and the correction factors. The total-gas, integrated and plateau ages also take into account the uncertainty in the flux-calibration parameter. All errors are given at the 95% confidence level. The ages were calculated using the IUGS-recommended constants (Steiger & Jäger, 1977).

GEOCHRONOLOGY

Previous work and new sampling strategy

Previously published K–Ar ages of the Brandberg (Watkins *et al.*, 1994) yielded a span of ages between 135·2 ± 1·5 and 125·4 ± 1·3 Ma. The apparent K–Ar ages of arfvedsonite from the Amis peralkaline granite were older than those of biotite and hornblende from the main massif, which contradicts the intrusive sequence based on field mapping. Armstrong *et al.* (1997) presented $^{206}Pb/^{238}U$ SHRIMP ages on zircons of an unspecified 'alkali ring-dyke' from the Brandberg massif (135 ± 1 Ma). This appears inconsistent with the fact that the Brandberg intruded Etendeka volcanic sequences, which have been dated by $^{40}Ar–^{39}Ar$ in the nearby Goboboseb area and elsewhere at 132 ± 1 Ma (Renne *et al.*, 1996). Renne *et al.* (1997) included unspecified Brandberg granitoids in a group of $^{40}Ar/^{39}Ar$ plateau ages at 132 ± 1 Ma, which they reported for Etendeka–Paraná intrusives.

In this study we present new $^{40}Ar/^{39}Ar$ dates for biotite, arfvedsonite and astrophyllite from three distinct evolutionary stages of the Brandberg complex. The main metaluminous granite intrusion is represented by two samples from the Numas valley (NU22 and NU30), far from the younger Amis intrusion, and therefore unlikely to have been thermally influenced by it. The subdivision of Diehl (1990) suggests that these samples belong to two distinct units: NU30 to an outer edenite–augite granite and NU22 to an 'edenite biotite ring dyke'. Three samples from the Amis complex cover the main peralkaline granite sill (AM206), a marginal peralkaline dyke (AM215) and secondary mineralization in segregations of aegirine–albite granite (AM219).

Results

The Ar-release patterns of three biotite separates from two main massif granite samples (Fig. 5) indicate considerable secondary loss of radiogenic Ar (7% for NU30, 13% for NU22), which results in total gas ages between 129·7 ± 0·7 Ma and 122·3 ± 0·7 Ma, respectively. These total gas ages have no geological meaning, and the observed radiogenic Ar loss would explain the age underestimate of conventional K–Ar dating of Watkins *et al.* (1994). Ages obtained for the intermediate to higher-temperature steps of the biotite release patterns (NU30 133·0 ± 0·8 Ma and NU22 132·6 ± 1·8 Ma) can be interpreted as minimum cooling ages and are indistinguishable within error for both samples. We conclude that the intrusive subdivisions suggested by Diehl (1990), if valid, cannot be resolved by $^{40}Ar–^{39}Ar$ dating.

The two arfvedsonite separates of peralkaline Amis granites yielded concordant plateau and total-gas dates that overlap within error (AM206 130·9 ± 0·7 Ma and AM215 132·0 ± 0·7 Ma). The calculated $^{40}Ar/^{39}Ar$ plateau age of the astrophyllite sample AM219 is 130·5 ± 0·7 Ma and, as in the biotite release patterns, some Ar loss is indicated by younger apparent ages for the low-temperature release steps (Fig. 5).

The Ar-release patterns of the amphiboles indicate rapid cooling and suggest that the plateau ages reported above represent realistic crystallization ages. The new data agree with the intrusive sequence inferred from field relations, and demonstrate the age equivalence of the sampled Brandberg units. Furthermore, these ages

Table 4: Selected chemical analyses of Brandberg metaluminous and peralkaline rocks

Sample:	GO07	GO10	B21a	B21d	AM71	AM67	AM61	NU40	NU37	NU30	NU22	B37	NU25 a
Unit:	td	td	m	m	mgr	mgr	mgr	mgr	mgr	mgr	mgr	blg	blg
Loc.:	Gom	Gom	Naib	Naib	Amis	Amis	Amis	Num	Num	Num	Num	Hun	Num
wt %													
SiO_2	66·8	66·9	61·5	63·6	68·7	70·9	70·4	68·0	70·6	68·9	71·9	76·8	76·4
TiO_2	0·93	0·92	1·46	1·05	0·31	0·46	0·52	0·62	0·45	0·60	0·40	0·14	0·07
Al_2O_3	13·3	13·4	13·6	14·5	15·2	13·2	13·2	13·4	12·9	13·2	13·1	12·3	12·3
Fe_2O_3*	6·69	6·70	9·68	7·12	3·07	3·92	4·59	5·85	4·23	5·38	3·37	1·48	0·93
Fe_2O_3	—	—	3·58	3·50	1·21	1·50	1·66	2·10	—	1·82	1·32	0·69	0·40
FeO	—	—	5·49	3·26	1·67	2·18	2·64	3·38	—	3·20	1·84	0·71	0·48
MnO	0·11	0·11	0·20	0·14	0·08	0·10	0·12	0·16	0·11	0·14	0·08	0·03	0·02
MgO	0·75	0·76	1·15	0·84	0·28	0·30	0·29	0·48	0·28	0·40	0·25	0·15	0·03
CaO	2·70	2·73	3·41	3·02	1·78	1·47	1·47	1·98	1·52	1·81	1·21	0·52	0·54
Na_2O	3·44	3·44	4·32	4·56	4·60	3·71	3·70	3·78	3·69	3·76	3·86	3·62	4·14
K_2O	4·37	4·42	3·64	4·04	5·03	5·28	5·09	4·79	5·06	4·89	5·25	5·17	4·82
P_2O_5	0·25	0·25	0·46	0·31	0·10	0·09	0·11	0·13	0·08	0·11	0·07	0·01	0·01
H_2O	0·29	0·39	0·77	0·74	0·28	0·31	0·39	0·55	0·36	0·39	0·29	0·15	0·20
CO_2	0·17	0·18	0·13	0·41	0·06	0·04	0·04	0·04	0·19	0·05	0·04	0·02	0·04
Total	99·83	100·21	99·71	99·97	99·51	99·75	99·97	99·78	99·44	99·64	99·74	100·31	99·42
ppm													
F	1400	1300	1180	—	660	1900	1200	1350	1450	1700	2400	3340	3750
Cl	—	—	—	—	290	210	430	310	—	320	260	—	110
Rb	146	146	144	140	186	206	212	186	207	193	279	408	568
Sr	200	201	225	240	273	111	112	147	118	118	96	19	10
Ba	914	902	747	869	1317	806	814	1017	772	835	739	129	15
Zr	366	358	373	391	523	398	412	396	399	473	363	212	144
Ga	23	23	25	26	24	24	25	26	25	24	23	24	28
Zn	100	91	156	108	65	97	108	109	132	143	85	32	51
Co	5·9	6·1	9·7	6·4	n.d.	2·1	n.d.	2·2	1·4	2·3	n.d.	0·3	n.d.
Sc	9·7	8·7	14	9·6	5·6	6·9	7·9	9·8	7·4	8·6	5·8	1·3	n.d.
Y	63	59	67	61	56	63	68	60	67	65	81	66	58
Nb	42	41	51	42	44	50	51	44	49	53	53	50	50
Cs	2·6	2·9	3·7	3	5·5	5·3	10	5·5	8·9	7·2	9·7	13	20
Ta	2·5	2·4	3·2	3	3·1	3·6	3·4	2·8	3·7	3·4	4	5·8	11
Pb	22	22	12	14	23	23	29	21	28	23	28	29	32
Th	23	22	14	16	18	27	19	19	24	21	28	45	75
U	5·2	5	5·1	4·6	3·2	6·0	9·6	6·2	4·8	4·6	6·7	13	36
La	71	68	68	56	62	73	67	73	82	63	76	67	39
Ce	145	134	134	116	123	165	143	147	166	133	140	132	66
Nd	64	61	61	53	55	66	65	66	74	62	63	47	16
Sm	13	12	12	11	11	13	14	13	15	14	13	9	3
Eu	2·4	2·3	2·3	3·4	3·1	2·2	2·6	3·1	2·5	2·6	2·0	0·6	0·1
Gd	12	11	11	12	11	12	13	13	14	13	12	9·3	2·5
Tb	2·1	2·0	2·0	1·8	1·7	2·0	2·1	2·0	2·2	2·1	2·3	1·8	0·5
Yb	6·0	5·5	5·5	6·1	5·5	6·4	6·7	6·3	7·0	6·9	7·6	8·3	4·3
Lu	0·9	0·9	0·9	0·9	0·8	1·0	1·0	1·0	1·1	1·0	1·2	1·3	0·7

Table 4: continued

Sample:	AM205b	AM206	AM207	AM208	AM209	AM215	AM61a	AM216	AM219
Unit:	am	am	am	am	am	am	am	am	am
Loc.:	Amis	Amis	Amis	Amis	Amis	Amis	Amis	Amis	Amis
wt %									
SiO_2	72·9	71·7	73·2	71·8	73·4	74·0	75·9	72·6	72·7
TiO_2	0·18	0·23	0·22	0·25	0·17	0·18	0·16	0·43	0·45
Al_2O_3	11·00	10·9	10·0	10·2	10·0	10·1	10·6	9·03	9·10
Fe_2O_3*	5·65	6·25	7·07	6·99	5·18	5·28	3·62	4·50	4·36
Fe_2O_3	2·73	2·75	3·05	2·90	2·31	—	—	4·26	3·09
FeO	2·63	3·15	3·62	3·68	2·58	—	—	0·22	1·14
MnO	0·08	0·09	0·09	0·09	0·06	0·06	0·05	0·04	0·11
MgO	0·04	0·02	0·02	0·04	0·05	0·03	0·01	0·02	0·01
CaO	0·18	0·05	0·02	0·03	0·15	0·14	n.d.	0·07	0·07
Na_2O	5·04	4·94	4·61	4·72	5·09	4·43	4·45	7·21	6·03
K_2O	4·37	5·05	4·79	4·87	3·64	4·53	4·33	0·06	1·61
P_2O_5	0·01	0·00	0·05	0·01	0·01	0·05	0·01	0·01	0·00
H_2O	0·18	0·21	0·35	0·24	0·24	0·26	0·15	0·12	0·15
CO_2	0·05	0·05	0·03	0·04	0·09	0·06	0·03	0·08	0·12
total	99·63	99·47	100·45	99·21	98·05	99·11	99·32	94·18	94·71
ppm									
F	5450	5050	4600	4850	5700	4050	2650	610	1650
Cl	400	n.d.	110	n.d.	n.d.	—	—	n.d.	n.d.
Rb	892	1102	891	992	966	1070	567	3·7	436
Sr	29	6·4	1·8	3·1	13	8·3	1·6	11	8·9
Ba	32	15	19	13	7	13	11	40	40
Zr	594	610	271	1247	4110	1289	2084	16800	12200
Ga	50	52	47	40	27	42	30	44	49
Zn	591	778	630	790	782	651	421	670	1480
Co	0·3	0·3	0·5	n.d.	n.d.	n.d.	n.d.	n.d.	n.d.
Sc	0·32	0·59	0·55	n.d.	n.d.	n.d.	n.d.	n.d.	n.d.
Y	509	395	37	282	844	151	21	1990	2170
Nb	92	556	30	302	413	214	276	2270	1520
Cs	6·9	12	8·1	10	14	11	8·2	0·57	37
Ta	6·9	33	1·4	25	33	15	—	93	66
Pb	14	220	10	92	148	99	16	303	976
Th	19	54	11	50	49	47	12	680	1120
U	12	59	1·9	39	57	24	32	187	124
La	241	209	124	170	480	131	8·9	309	301
Ce	514	501	325	422	954	301	58	769	763
Nd	302	190	93	178	660	121	15	423	436
Sm	83	48	20	50	173	22	4·1	145	156
Eu	2·2	1·2	0·5	1·3	4·4	0·4	0·1	4·5	4·9
Gd	91	47	15	58	208	16	3·7	189	206
Tb	13	8	2·3	11	28	3·0	0·8	42	50
Yb	21	28	9·2	28	50	19	4·1	176	254
Lu	3·1	4·2	2·0	4·2	7	2·9	0·6	22	32

Rock units: td, trachydacite; m, monzonite; mgr, main hornblende–biotite granite; blg, biotite leucogranite; am, Amis peralkaline granite. Loc. (sample location): Gom, Gomatsarab; Num, Numas valley; Hun, Hungorob valley. —, not analysed; n.d., not detectable. GPS coordinates available on request. Fe_2O_3* is total Fe as Fe_2O_3.

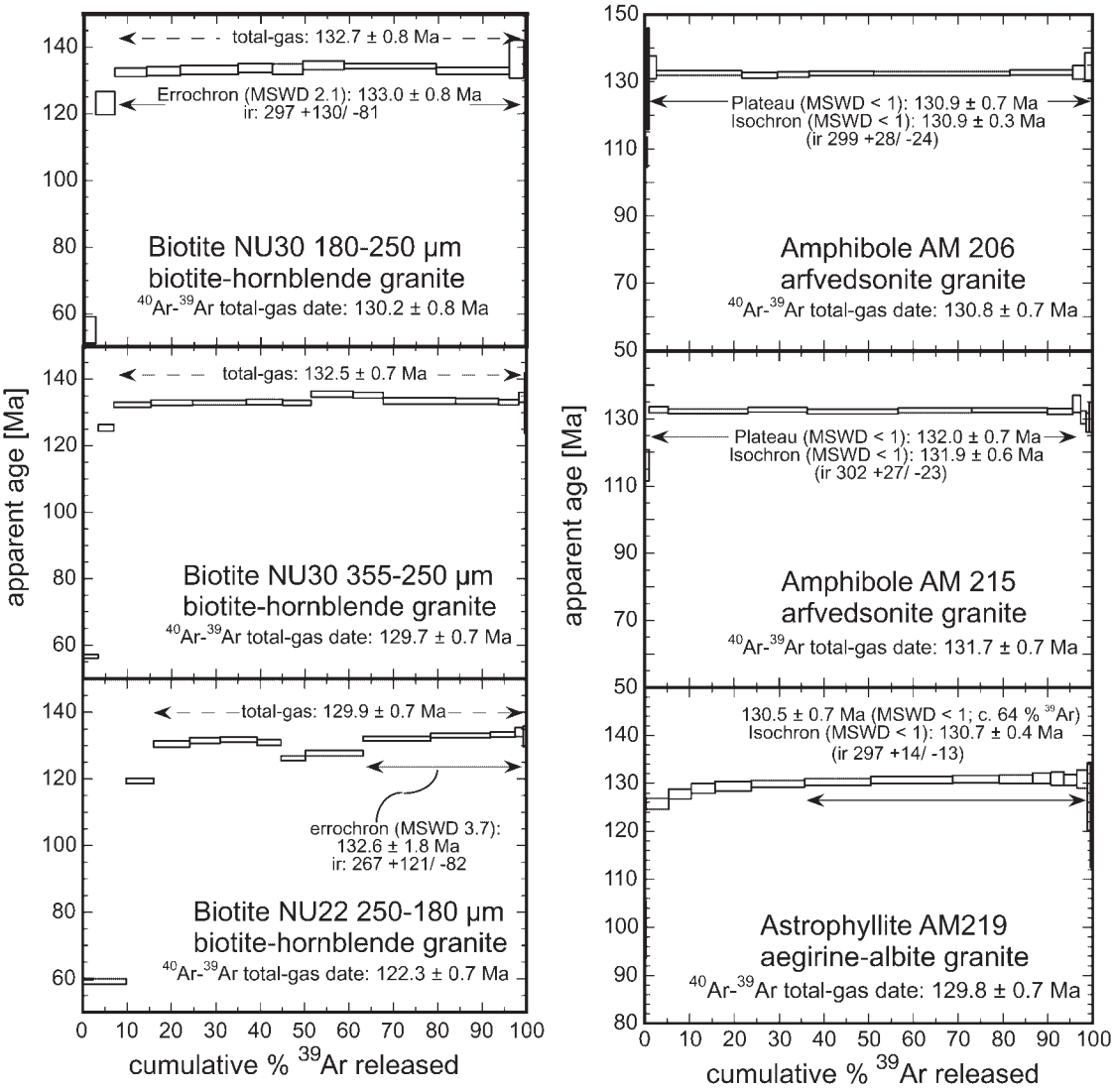

Fig. 5. $^{40}Ar/^{39}Ar$ apparent age spectra for metaluminous and peralkaline samples from the Brandberg complex located in Fig. 1. ir, initial $^{40}Ar/^{36}Ar$ ratio.

closely overlap the span in ^{40}Ar–^{39}Ar ages of the nearby Messum complex (132·1 ± 0·7 Ma to 129·3 ± 0·7 Ma, Renne *et al.*, 1996) and the K–Ar ages of the Okenyenya complex (133·3 ± 0·7 Ma to 129·2 ± 0·7 Ma, Watkins *et al.*, 1994). The Brandberg data indicate a remarkably short duration of magmatic activity, probably <1 My. Even the astrophyllite from mineralized aegirine–albite segregations in the Amis complex is indistinguishable in age from the clearly magmatic arfvedsonite granites.

Therefore, the age of the Brandberg complex coincides with the peak activity of the Etendeka province, as recently defined by ^{40}Ar–^{39}Ar ages and palaeomagnetic data (Renne *et al.* 1996), and reinforces the concept of rapid emplacement of both intrusive and extrusive magmas between 133 and 130 Ma.

WHOLE-ROCK GEOCHEMISTRY AND ISOTOPIC COMPOSITION

Variation diagrams for selected major elements, and compatible and incompatible trace elements plotted against FeO* (total Fe as FeO) are shown in Fig. 6. Table 4 gives representative whole-rock chemical compositions of the igneous units from the Brandberg complex. An effective chemical division for the Brandberg rocks is their molar (Na + K)/Al ratio, which

distinguishes a metaluminous and a peralkaline group (Fig. 6a and i). Both groups form two subparallel trends in the SiO_2–FeO* variation diagram with an overlap in SiO_2 between 70 and 75 wt % and a general negative correlation between SiO_2 and FeO* (Fig. 6b and j). The metaluminous group includes all units of the main massif (monzonite, hornblende–biotite granite and leucogranite) as well as the peripheral trachydacite dykes. The peralkaline group consists of different textural varieties of arfvedsonite and aegirine granites from the Amis satellite intrusion. Haematized arfvedsonite granites may have (Na + K)/Al <1 as a result of the postmagmatic replacement of Na-bearing arfvedsonite by quartz and haematite and are therefore not considered further.

Metaluminous group (main massif and peripheral dykes)

The rocks of the metaluminous group cover a total range of SiO_2 from 61 to 77 wt %. With decreasing FeO*, the molar ratio of (Na + K)/Al increases from ~0·8 to unity, whereas this ratio in the peralkaline group ranges from 1·0 to 1·5. The metaluminous samples have all the chemical characteristics of A-type granites according to the compilations of Whalen *et al.* (1987), particularly the high Ga/Al ratios. Fluorine contents are also high (average 1500 ppm for hornblende–biotite granite) compared with those of orogenic granitoids (Christiansen & Lee, 1986).

Systematic chemical variations occur in samples from the Naib valley monzonite, trachydacite dykes and granite of the main massif. These can be best illustrated using FeO* as a differentiation index. With decreasing FeO*, contents of TiO_2, MgO, CaO and P_2O_5 decrease, Al_2O_3 and K_2O remain nearly constant, and SiO_2 and Na_2O increase. As an example, Fig. 6 illustrates the regular variation trends of SiO_2, TiO_2 and CaO against FeO* for the Brandberg metaluminous suite. It also shows the overall similarities of the trachydacites and least evolved biotite–hornblende granites with felsic volcanics of the Etendeka–Paraná, in particular for major element composition.

Smooth trends with no break in slope are observed for elements compatible in feldspar and pyroxene or amphibole such as Sr (also Ba, Zn and Sc, not shown). Incompatible elements such as Rb and F systematically increase with decreasing FeO*. Pairs of incompatible elements in the biotite–hornblende and biotite granites have constant ratios, such as Rb/Th (~9, linear correlation factor $r = 0{\cdot}89$), Rb/U (~34, $r = 0{\cdot}88$) and Rb/Cs (~32, $r = 0{\cdot}84$), suggesting that fluid overprinting and alteration is insignificant. Other trace elements such as Zr (and Y not shown) display a kinked trend with differentiation. Contents of Zr first rise slightly and then fall with differentiation, probably as accessory minerals such as zircon enter the fractionating assemblage at FeO* contents of ~3·5 wt %.

All units of the metaluminous group show very similar variation in chondrite-normalized REE distributions up to ~5 wt % FeO* (Fig. 7), with gently sloping patterns ($La_n/Lu_n = 5{\cdot}8$–$7{\cdot}8$). The slight increase of La_n/Lu_n with decreasing FeO* that is observed for the monzonite–biotite–hornblende granite suite is consistent with clinopyroxene present within the fractionating assemblage. In keeping with other fractionation indicators such as decreasing Sr or increasing Rb, the more evolved granites have lower overall REE abundances, lower light REE to heavy REE (LREE/HREE) ratios ($La_n/Lu_n = 6{\cdot}6$–$5{\cdot}3$) and a more pronounced negative Eu anomaly; the ratio of Eu/Eu* decreases from 0·95–0·7 in the least evolved rocks (trachydacite, monzonite, hornblende–biotite granites) to 0·17 in the leucogranites (Eu* is the mean of Gd + Sm, with all values chondrite normalized). Feldspar fractionation can account for the relative Eu depletion, whereas decreasing LREE/HREE ratios, commonly observed in evolved high-Si rock suites, are attributed to fractionation of accessory phases (e.g. monazite, chevkinite).

The close temporal and spatial relation between the emplacement of the Brandberg granites and the eruption of the Etendeka quartz latites suggests that they might be related to the same magmatic event. Best suited for testing a direct correlation between the Brandberg subvolcanic complex and Southern Etendeka felsic extrusives are the trachydacite dykes, which resemble the quartz latites in terms of mineralogy, texture and major element composition. Milner & Duncan (1987) derived discriminant functions from whole-rock major and trace element variables to distinguish different quartz latite units in Namibia. When applied to the trachydacite dykes, this method indicates a clear difference in bulk composition from any of the quartz latites examined by Milner & Duncan (1987). Figure 8 presents normalized incompatible trace element data from trachydacite dykes and Brandberg granite along with published compositions of the quartz latites (Awahab Formation) and correlated Paraná low-Ti rhyodacites of the Palmas type (Milner *et al.*, 1995*a*). All samples plotted have SiO_2 contents of 65–70 wt %, with the exception of the Brandberg monzonite (62 wt %). The comparison shows that the trachydacite and Brandberg granites are compositionally similar to one another and can be distinguished from the felsic volcanics. In detail, the Brandberg felsic rocks have higher Ba, Th, Nb, Ta, Zr and REE than the average Etendeka low-Ti quartz latites. Although we compare values from different laboratories and analytical techniques, the differences (>25% relative for Zr, Nb and La) are independent of the techniques used and greatly exceed

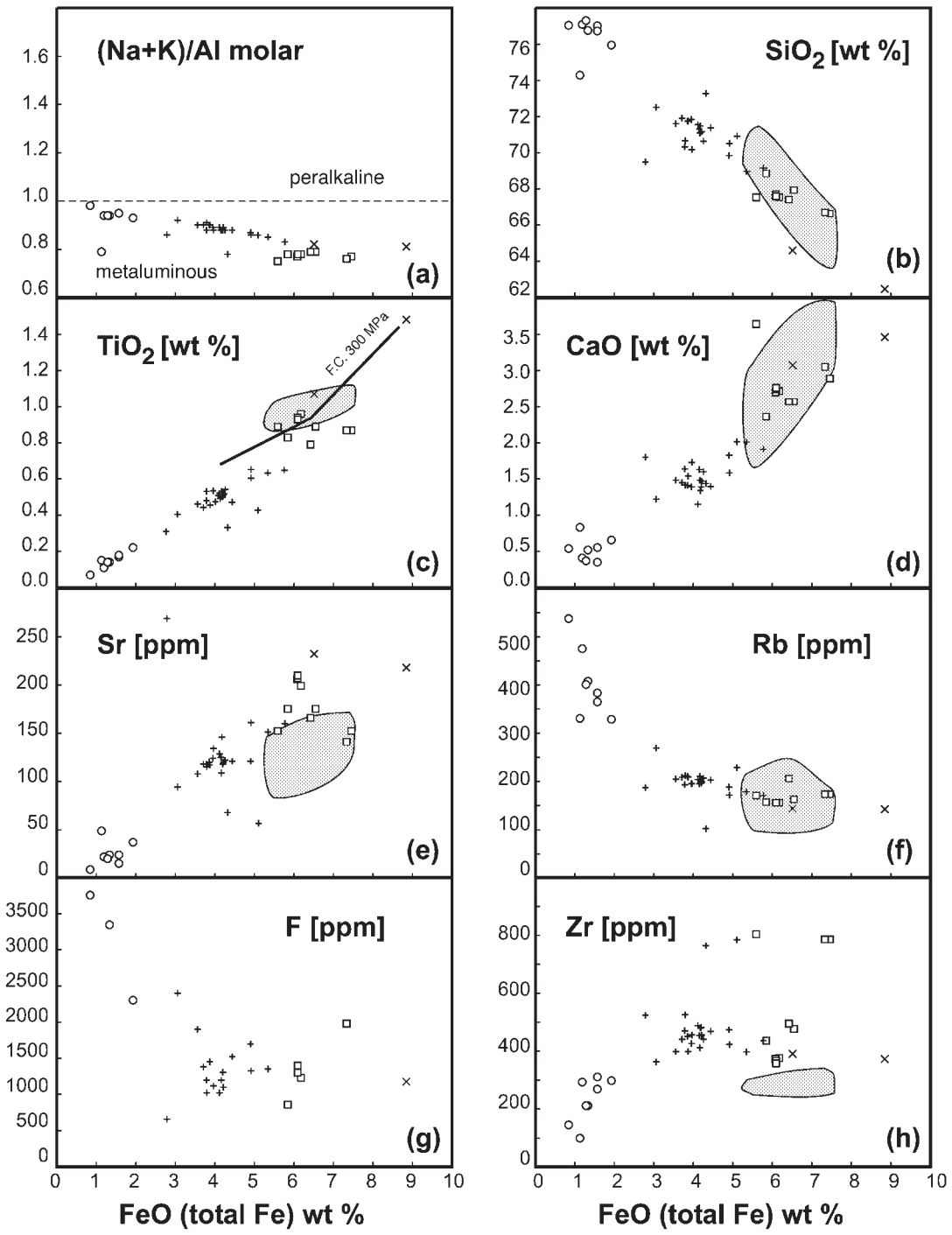

Fig. 6.

analytical variations commonly observed from analysis of international reference materials (Govindaraju *et al.*, 1994). The Sr and Nd isotopic data underscore these differences (see below).

Peralkaline granites: the Amis complex

The best estimate of peralkaline granite magma composition unaffected by mineral segregation and subsolidus changes may be given by analyses of fine-grained

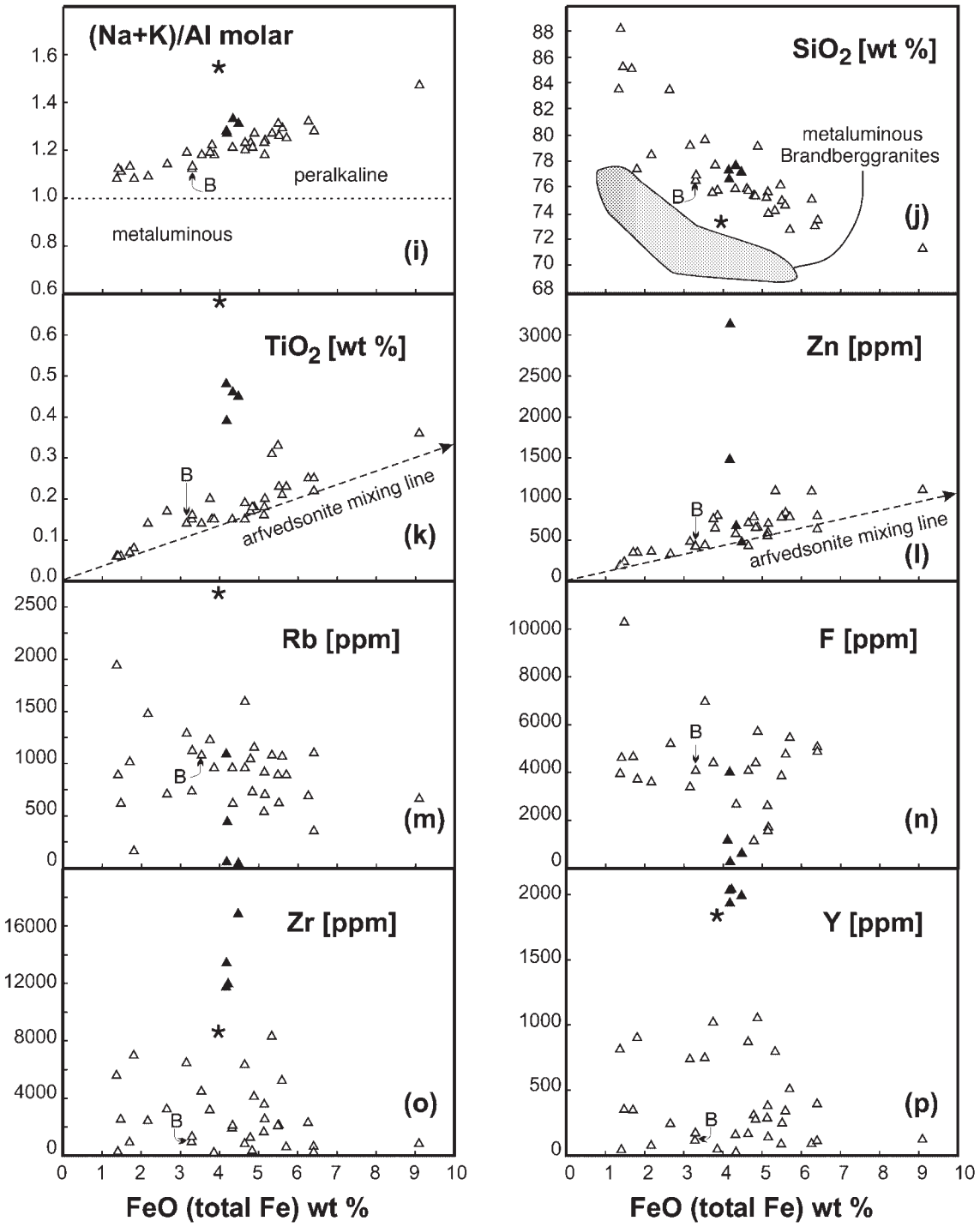

Fig. 6. (a–h) Variation diagrams for metaluminous rocks of the Brandberg using FeO* as a differentiation index (×, monzonite; □, trachydacite dykes; +, biotite–hornblende granite; ●, biotite leucogranite). Fields for Etendeka–Paraná basic to acid lavas are shown for comparison (Garland *et al.*, 1995; Ewart *et al.*, 1998*b*). (c) shows the MELTS fractional crystallization line for 300 MPa (1 wt % H_2O, QFM oxygen buffer, $T_{liquidus}$ = 1107°C). Modelling using same conditions for 1000 MPa indicates a divergent TiO_2 enrichment trend with decreasing TiO_2 up to 1·9 wt % at FeO* = 6 wt %. (i–p) Variation diagrams of selected major and trace elements against FeO* of Amis peralkaline granites (△, arfvedsonite granite; ▲, aegirine–albite granites; B, arfvedsonite granite dyke 'Brandbergite' AM61a; ★, average melt inclusion composition). Arfvedsonite mixing line drawn using Fe-, Ti- and Zn-free quartz–feldspar association and average arfvedsonite composition determined by electron microprobe (FeO* = 33 wt %, TiO_2 = 0·9 wt %, Zn = 1000 ppm) as end-members.

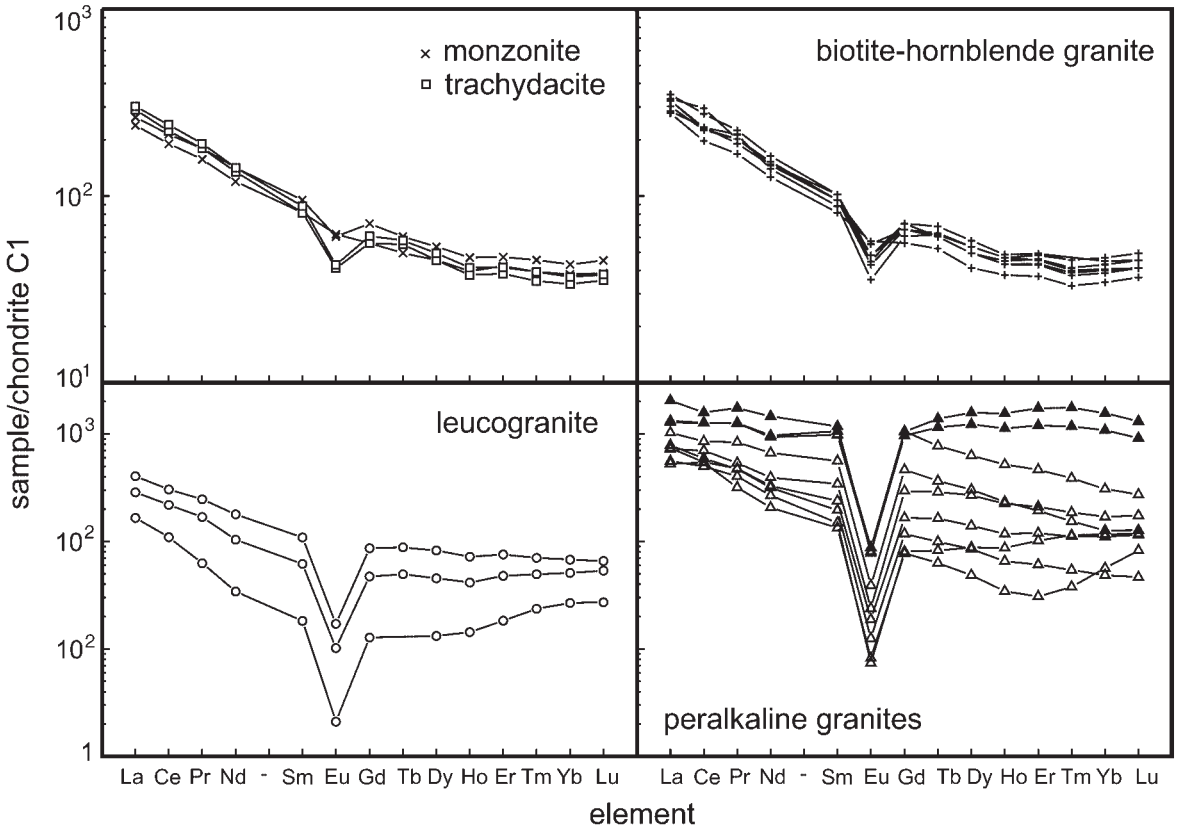

Fig. 7. Chondrite-normalized REE patterns of metaluminous and peralkaline rocks of the Brandberg; symbols as for Fig. 6 [C1 chondrite after Anders & Grevesse (1989)].

peralkaline dykes ['Brandbergites' of Cloos & Chuboda (1931)]. Liquid compositions can also be derived directly, in some samples, by analysis of rehomogenized melt inclusion glasses. Melt inclusions have so far been measured only from pegmatitic phases of the peralkaline granites and are regarded as an indicator for the late-stage residual melts. The data document high levels of HFSE enrichment in residual melts of the peralkaline granite. Table 5 shows electron microprobe analyses of the glass phase of heated melt inclusions from pegmatitic quartz in which extreme levels of F, Zr, Y and Ce occur.

The peralkaline granites tend to higher silica values than the metaluminous group (total range 70–88 wt % SiO_2, average 76 wt %). In a FeO*–SiO_2 diagram (Fig. 6j), the samples show a variation trend that is consistently displaced to higher FeO* contents compared with the metaluminous trend ($\sim$2 wt % at a given SiO_2 value; see Fig. 6b). Interpretation of the compositional variations in the peralkaline granites encounters three major difficulties. First, the granites are strongly layered in outcrop, with cumulative mineral enrichments and large variations in modal arfvedsonite. Second, interstitial accessory minerals rich in trace elements are unevenly distributed and affect whole-rock trace element patterns. Thirdlt, there is petrographic evidence for late-stage mineral replacements and secondary quartz growth, particularly in haematized granites, where arfvedsonite has been completely replaced by quartz and haematite. We therefore discarded samples showing evidence of mineral replacements and alteration based on petrographic and modal compositional data. Nevertheless, the problem of representative sampling remains and we are aware of the problems in interpreting the data as representing liquid compositions.

Figure 6(i–p) illustrates selected major and trace element variations in peralkaline granites plotted against FeO*. The wide range in FeO* (and positively correlated major and trace elements such as TiO_2, MnO, Zn and Sc) is inferred to be largely controlled by the modal abundance of arfvedsonite as demonstrated by the mixing line shown in Fig. 6(k and j). It should be noted that the fine-grained dyke rocks ('Brandbergites'), which can be expected to represent liquid compositions, correspond to an intermediate granite composition in the variation diagrams.

Summing up, the overall chemical characteristics of the peralkaline Amis suite [besides its (Na + K)/Al >1]

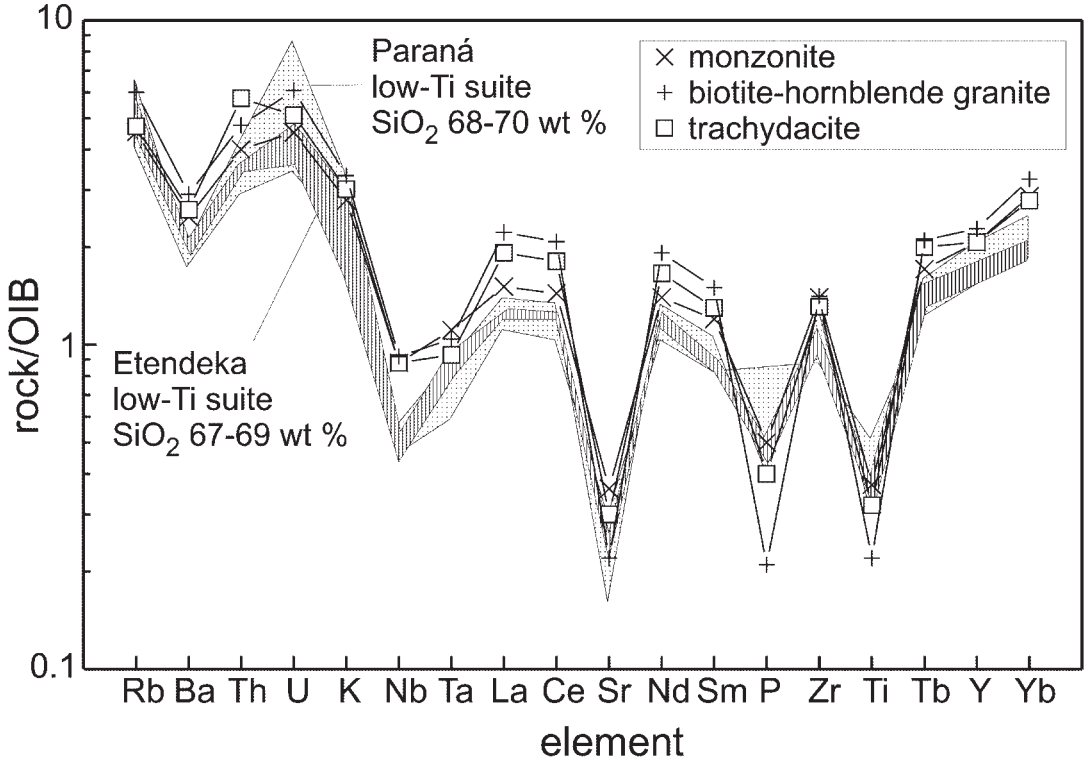

Fig. 8. OIB-normalized trace elements of Brandberg metaluminous rocks compared with low-Ti felsic volcanics from the Paraná province (Garland *et al.*, 1995) and Etendeka (Ewart *et al.*, 1998*b*). Normalizing values from Sun (1980) cited by Rollinson (1993).

are high FeO*/Al_2O_3, low MgO and CaO, high Ga/Al and high enrichments in incompatible elements (e.g. Rb and HFSE). At a given FeO* value, peralkaline granites tend to have higher SiO_2 compared with the metaluminous rocks. Compared with the most differentiated metaluminous leucogranites from the main massif, the peralkaline rocks are depleted in Al_2O_3, K_2O, MgO, CaO, Sr and Ba, and richer in TiO_2, MnO, Na_2O, F and the incompatible lithophile elements (Rb, Pb, Th, U, Nb, Ta, Zr and Y). There is a striking contrast between the metaluminous and peralkaline groups in terms of a number of incompatible elements (F, Y, Zr, REE, U and Th), whose magmatic abundance is controlled by accessory mineral stability. The highest measured HFSE contents (2900 ppm Nb, 1·7 wt % Zr, 2000 ppm Y) were found in dyke-like segregations of aegirine–albite–quartz rocks. These rocks contain a complex accessory mineral assemblage including many late interstitial phases and mineral overgrowths; this feature indicates that the present rock does not represent entirely magmatic compositions.

Further evidence for the extreme degree of fractionation of the peralkaline granites is that they have the most pronounced negative Eu anomaly of all Brandberg rocks (Fig. 7), with a value of Eu/Eu* of only 0·1, compared with a minimum of 0·17 for the leucogranites from the main massif. Unlike the metaluminous group, total REE abundances in the peralkaline granites increase with a more negative Eu anomaly resulting from feldspar fractionation.

Two samples of aegirine–albite–quartz rocks have the highest total REE contents and chondrite-normalized LREE to HREE ratios close to unity. The chondrite-normalized REE patterns display slightly kinked shapes with minima at Nd and Ho. This so-called tetrad effect is typical for highly evolved leucogranites and pegmatites, and has been attributed to selective complexation behaviour of REE in very fluid-rich melts (Bau, 1996).

Sr and Nd isotopes

The Sr and Nd isotopic compositions of samples from the metaluminous units are listed in Table 6 and shown in Fig. 9 together with other data from Cretaceous igneous complexes in Namibia and with selected mixing and AFC models discussed in a later section. The isotopic values (all recalculated to an age of 130 Ma) cover a considerable range and this demonstrates at the outset that the metaluminous group as a whole cannot be considered a closed-system differentiation series (see also petrogenetic modelling section below). Uncertainties in

Table 5: Summary of electron microprobe analyses of melt inclusions (n = 10) in quartz from the Amis peralkaline granite (in wt %)

	Mean	*Standard deviation*
SiO_2	66·9	1·0
TiO_2	0·63	0·14
Al_2O_3	9·14	0·12
FeO	3·66	0·34
MnO	0·16	0·03
MgO	<0·05	
CaO	<0·05	
Na_2O	5·12	0·23
K_2O	5·29	0·28
F	4·60	0·5
Cl	0·17	0·08
ZrO_2	1·09	0·07
Y_2O_3	0·23	0·08
Ce_2O_3	0·14	0·05
Rb_2O	0·36	0·03
P_2O_5	0·05	
–O=F	−2·02	
Total	95·68	
NK/A	1·59	

the age of the intrusion (130 ± 2 Ma) have no significant effect on the calculated initial Sr isotopic ratios of the biotite granite.

Within the main massif granites, isotopic variation is insignificant within error. Values for five samples of the hornblende–biotite granite are $\varepsilon Nd_{(130\,Ma)} = -2{\cdot}8$ to $-3{\cdot}3$ and $^{87}Sr/^{86}Sr_{(130\,Ma)} = 0{\cdot}7117$–$0{\cdot}7132$. A biotite leucogranite (B37 in Table 6) from the main massif yields a value of $\varepsilon Nd_{(130\,Ma)} = -2{\cdot}4$, consistent with the interpretation that the leucogranite is a differentiated facies of the hornblende–biotite granite. Because of its high Rb/Sr ratio, the initial $^{87}Sr/^{86}Sr$ ratio of this sample (0·727 ± 0·05) is too imprecise to be a useful constraint, but overlaps within error with the range of the hornblende–biotite granites. Two units of the metaluminous group deviate significantly from the main massif granites in terms of isotopic composition. The Naib valley monzonite has rather primitive isotopic ratios, with $\varepsilon Nd_{(130\,Ma)} = -0{\cdot}5$ to $-0{\cdot}8$ and $^{87}Sr/^{86}Sr_{(130\,Ma)} = 0{\cdot}7072$–$0{\cdot}7085$ ($n = 2$). The peripheral trachydacite dykes ($n = 2$) have less radiogenic Nd ratios than the main massif, with $\varepsilon Nd_{(130\,Ma)} = -4{\cdot}9$ to $-5{\cdot}1$, whereas the $^{87}Sr/^{86}Sr_{(130\,Ma)}$ values, 0·7131–0·7132, overlap with those of the main massif.

Because of the extremely high Rb/Sr ratios of the peralkaline granites (up to 500), calculated initial $^{87}Sr/^{86}Sr_{(130\,Ma)}$ values are too imprecise for any petrogenetic conclusions. The only sample with a moderate Rb/Sr ratio (AM216 in Table 6) yielded an initial Sr value of ~0·710, which overlaps with those of the metaluminous group. However, the Nd isotopic compositions of the peralkaline granites, with $\varepsilon Nd_{(130\,Ma)}$ in the range from $-0{\cdot}7$ to $-1{\cdot}9$, differ significantly from those of the main massif granites and trachydacite, and most samples are more similar to the values of the Naib valley monzonite.

DISCUSSION

P–T conditions and magmatic water concentrations

A number of methods to calculate magmatic temperatures can be applied to the Brandberg rocks but the mineral assemblages do not permit a reliable estimate of pressure. In particular, hornblende compositions from the biotite–hornblende granite belong to the low-fO_2 series of Anderson & Smith (1995), which are too low in $Fe^{3+}/(Fe^{2+} + Fe^{3+})$ (0·20–0·24) and too high in $Fe_{tot}/(Fe_{tot} + Mg)$ ratios (0·73–0·85) compared with the limits for compositions suitable for Al-in-hornblende barometry [>0·25 and 0·40–0·65, especially; see Anderson & Smith (1995)].

Geological evidence clearly indicates a very shallow level of emplacement. Roof pendants at the top of the Brandberg massif are lavas, and the Brandberg granite intrudes essentially coeval surficial lava flows (Etendeka Group) around its margins. An indirect estimation of crystallization pressure emerges from comparison of observed and modelled fractional crystallization paths, which were modelled using the MELTS software (Ghiorso & Sack, 1995) for a parental monzonite (assuming fO_2 buffered by QFM; 1 wt % H_2O). The modelled low-pressure (300 MPa) fractionation path compares well with the observed variations in the range of FeO* between 9 and 5 wt %. By contrast, high-pressure fractionation at 1000 MPa yields only a poor fit, especially for TiO_2 (see Fig. 6c).

Another semi-quantitative estimation of the late-stage evolution of the metaluminous magma can be obtained using the normative quartz, albite and orthoclase projection for primitive and evolved leucogranites and the modelled fractionating phase assemblage. These plot along the low-pressure quartz–orthoclase cotectic line in the water-saturated haplogranitic system (Winkler, 1979), suggesting final equilibration of these magmas at a shallow depth.

Application of the two-pyroxene thermometer of Lindsley (1983) to the trachydacite dykes yields a temperature for equilibration between pigeonite and augite

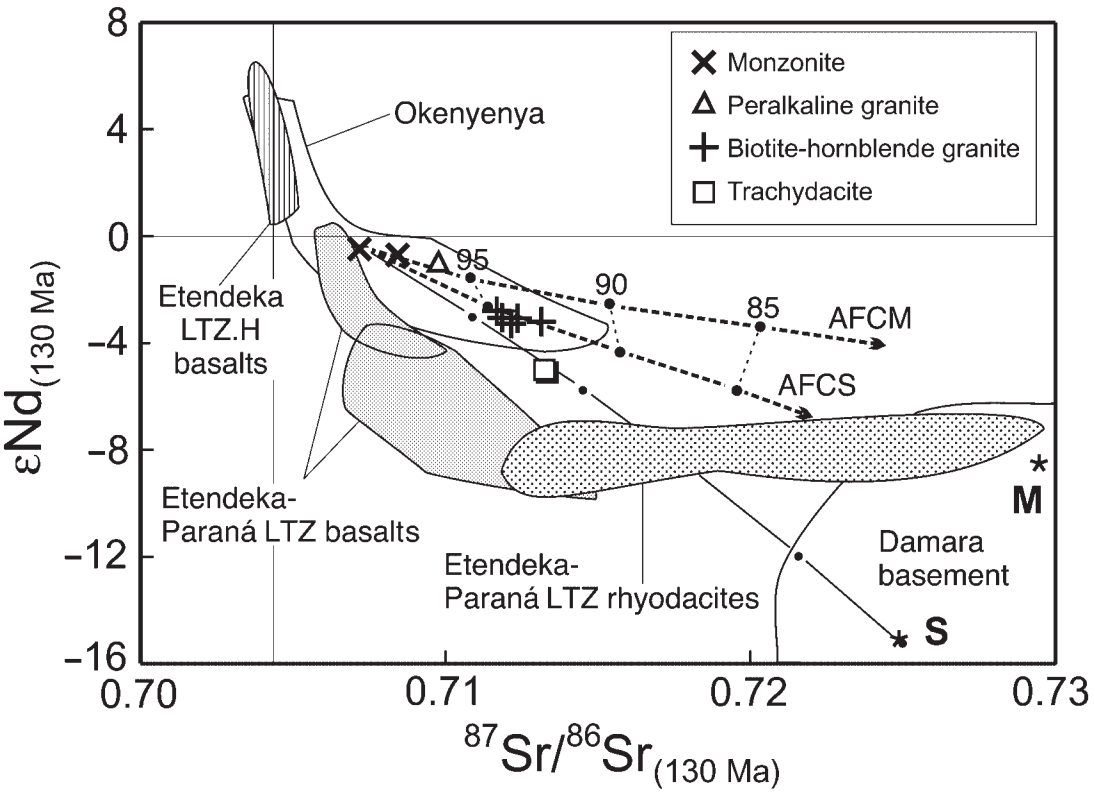

Fig. 9. Initial Nd–Sr isotopic composition of the Brandberg metaluminous rocks. For comparison, data for Etendeka–Paraná LTZ basalts (upper field, Esmeralda-type from Brazil; lower field, Etendeka and Gramado-type from Brazil) and rhyodacites (Erlank *et al.*, 1984; Garland *et al.*, 1995; Peate & Hawkesworth, 1996), Messum and Goboboseb lavas (including LTZ.H basalts) (Ewart *et al.*, 1998*a*) and the Okenyenya gabbroic complex (Milner & le Roex, 1996) are shown (all values calculated at 130 Ma). Upper field for LTZ basalts. The similarity of Brandberg and Okenyenya isotope ratios and dissimilarity with the Etendeka–Paraná flood basalt rocks should be noted. Field for Damaran basement from McDermott & Hawkesworth (1990) and McDermott *et al.* (1996), with calculated average greywacke-type metasedimentary (M) and Salem granite (S) isotopic composition. Dashed lines show calculated crust–mantle AFC trends using a monzonitic end-member composition and parameters from Table 7. Continuous line is calculated mixing trend between parental monzonite and basement S. Dots along the curves represent steps in f of 5% for AFC and 20% mixing intervals, respectively.

phenocrysts of about 970 ± 30°C, which is ~100°C lower than temperature estimates for the Awahab quartz latites using the same method (Ewart *et al.*, 1998*b*). Zircon saturation thermometry based on the experimental data of Watson & Harrison (1983) yields minimum temperatures of 850–880°C for the hornblende–biotite granites of the main massif. The LREE (monazite) saturation thermometer of Montel (1993) is a function of both temperature and water content. If temperature is known from an independent method, the monazite thermometer can be used to estimate magmatic water contents. When applied to samples of the hornblende–biotite granite that contain both monazite and zircon, the monazite thermometer yields temperatures concordant with the zircon and pyroxene thermometry for water concentrations of 1–3 wt %. We conclude from these results that the Brandberg metaluminous granites crystallized from a relatively hot magma and that primary magmatic water contents were relatively low.

Oxygen isotope data on coexisting quartz [$\delta^{18}O$ (SMOW) = 10·8‰] and pyroxene–amphibole [$\delta^{18}O$ (SMOW) = 7·6‰] in a peralkaline dyke ('Brandbergite') are consistent with equilibrium at magmatic temperatures (Harris, 1995; C. Harris, personal communication, 1999). This suggests that the role of fluid processes was greatly overemphasized by Diehl (1990). Electron microprobe glass analysis of quartz-hosted melt inclusions from peralkaline pegmatites yielded estimates of 4·3 wt % H_2O (difference of analytical total from 100 wt %) and high F contents of 4·6 wt % (Table 5). These values have to be considered as minimum estimates, as the design of the homogenization experiment was to homogenize inclusions rapidly with low experimental effort. One consequence of this is that there might have been volatile loss. Nevertheless, these data indicate that the residual peralkaline melt was relatively rich in volatiles, which is also supported by field evidence suggesting a low-viscosity magma.

Table 6: Nd and Sr isotopic compositions of whole-rock samples from the Brandberg complex

Sample	Unit	$^{147}Sm/^{144}Nd$	$^{143}Nd/^{144}Nd$	$^{143}Nd/^{144}Nd_{(130)}$	$\varepsilon Nd_{(130)}$	$^{87}Rb/^{86}Sr$	$^{87}Sr/^{86}Sr$	$^{87}Sr/^{86}Sr_{(130)}$
GO07*	td	0·122	0·51231	0·51221	−5·1	2·11	0·71709	0·71319
GO10*	td	0·118	0·51232	0·51222	−4·9	2·10	0·71699	0·71310
B21a*	m	0·132	0·51255	0·51243	−0·7	1·85	0·71191	0·70849
B21d*	m	0·134	0·51256	0·51245	−0·4	1·69	0·71038	0·70726
AM71*	mgr	0·127	0·51241	0·51231	−3·2	1·97	0·71592	0·71228
AM67*	mgr	0·122	0·51244	0·51234	−2·6	5·38	0·72195	0·71202
AM61*	mgr	0·135	0·51242	0·51231	−3·2	5·48	0·72336	0·71323
NU40*	mgr	0·122	0·51243	0·51232	−2·9	3·66	0·71842	0·71165
NU30*	mgr	0·128	0·51244	0·51233	−2·8	4·74	0·72044	0·71168
B37*	blg	0·117	0·51245	0·51235	−2·4	49·22	0·81806	0·72712
AM61A*	am	0·267	0·51254	0·51241	−1·4	—	—	—
AM205b†	am	0·163	0·51256	0·51242	−1·0	84·47	0·89249	—
AM206†	am	0·152	0·51256	0·51243	−0·8	468·40	1·50879	—
AM207†	am	0·127	0·51248	0·51237	−1·9	926·50	3·07408	—
AM208†	am	0·157	0·51253	0·51240	−1·4	1302·00	2·88393	—
AM209†	am	0·158	0·51257	0·51243	−0·8	215·10	1·04543	—
AM215†	am	0·111	0·51252	0·51242	−1·0	421·80	1·41564	—
AM216†	am	0·206	0·51261	0·51243	−0·7	0·99	0·71175	0·70992

*Sm, Nd by ICP-MS; Rb, Sr by XRF.
†Sm, Nd, Rb, Sr by isotope dilution; 2σ precision of $^{143}Nd/^{144}Nd$ and $^{87}Sr/^{86}Sr$ is better than 0·0001.
Rock units: td, trachydacite dykes; m, monzonite; mgr, hornblende–biotite granite; blg, biotite leucogranite; am, Amis peralkaline granite. Values used for calculations: present-day values for bulk Earth: $^{143}Nd/^{144}Nd = 0·51264$, Sm/Nd = 0·324, $^{87}Sr/^{86}Sr = 0·7047$, Rb/Sr = 0·032.

Source constraints

Crustal components

Potential crustal sources in the basement of the Damara Orogen include (1) pre-Damara rocks, (2) metasedimentary sequences of the Damara Orogen and their anatectic products, and (3) more primitive Pan-African I- and A-type granites.

Pre-Damara basement rocks occur in tectonic inliers in the northern Damara Belt and Kaoko Belt. Nd and Sr isotopic data from the late Archaean and early Proterozoic felsic gneisses and granitoids cropping out in the Kaoko Belt of NW Namibia (Seth *et al.*, 1998; B. Seth, personal communication, 1999) yielded εNd values from −26 to −31 at 130 Ma and initial $^{87}Sr/^{86}Sr$ ratios from 0·711 to 0·730. Similar rocks, with εNd values between −18 and −22 at 130 Ma, have been described from the São Francisco craton on the Brazilian margin (Garland *et al.*, 1995). If these values are typical for the pre-Damara crust, then its contribution to the source of the Brandberg granites (εNd = 0 to −3) can only be minor.

The Pan-African crust of the Damara Belt, judging from the most deeply eroded Central Zone, is dominated lithologically by medium- to high-grade metasediments and late- to post-tectonic peraluminous (S-type) granites. Previous studies of these units have demonstrated that the granites are isotopically similar to the metamorphic rocks (Haack *et al.*, 1983; McDermott & Hawkesworth, 1990; McDermott *et al.*, 1996). When recalculated to 130 Ma, both the Damara metasediments and the peraluminous granites have $^{87}Sr/^{86}Sr$ ratios exceeding 0·72 and values of εNd less than −7, which are considerably different from the corresponding ratios in the Brandberg granites (see Fig. 9). This conclusion also holds for a hypothetical melt-depleted equivalent of the metasediments, as their $^{87}Sr/^{86}Sr$ initial ratio at 500 Ma already exceeds the Brandberg initial ratio of 0·712, and the εNd values of the Brandberg at 130 Ma are higher than any restite composition with a reasonable Sm/Nd (Vervoort & Patchett, 1996) that has εNd values less than −7 at 500 Ma.

Isotopically more primitive Pan-African granitoids are not common in the Damara Belt but they do exist. Examples that have been characterized isotopically include I-type diorites and granodiorites reported by Hawkesworth *et al.* (1981) and Haack *et al.* (1983), and A-type leucogranites recently studied by Jung *et al.* (1998).

The εNd and initial Sr ratios of these granitoids calculated at 130 Ma are −4·5 and 0·706, respectively, for the diorites and −4 to −10 and 0·715–0·722, for the A-type plutons. Even these granitoids, then, are isotopically less primitive than the Brandberg initial ratios.

On the basis of these data, we can conclude that none of the Pan-African basement lithologies, nor the pre-Damara crust, could be the sole source of the Brandberg granites.

Mantle components

Constraints on the mantle components likely to be involved in magma genesis of the Brandberg complex are given by data from the coeval Etendeka flood basalts and related basic intrusions such as Messum and Okenyenya. Two compositionally distinct groups of flood basalts are distinguished regionally in the Etendeka and Paraná sequences, one relatively rich in Ti and HFSE (high Ti–Zr or HTZ group) and the other with lower concentrations of those elements (low Ti–Zr or LTZ group). The two groups are separated geographically in Namibia, and the Brandberg is located in the region dominated by LTZ basalts (Fig. 1). The basalts closest to the Brandberg intrusion (Goboboseb mountains) display two contrasting varieties (Ewart *et al.*, 1998*a*). One is similar to the typical low-Ti Etendeka–Paraná type, and has isotopic ratios (εNd = −6·1 to −8·5 and Sr_i = 0·708–0·716) that Ewart *et al.* suggested to result from crustal contamination. The second type of basalt (LTZ.H) has higher HFSE concentrations than typical low-Ti basalt, and it has distinctive isotopic and trace element characteristics, which Ewart *et al.* (1998*a*) attributed to a mantle plume source. The total range in Nd and Sr isotopic composition reported from the LTZ.H basalts is considerable (εNd from +6 to +1 and Sr_i from 0·704 to 0·705). A similar range of isotopic compositions, but extending to lower εNd values (e.g. εNd from +5 to zero), has been reported from alkali gabbros and nepheline syenites from the Okenyenya complex for which a mantle-plume origin was inferred (Milner & le Roex, 1996). Gabbros and syenites from the nearby Messum complex have yielded εNd values of −3 to +4 and Sr initial ratios of 0·704–0·710 (Trumbull *et al.*, 1997; Trumbull *et al.*, unpublished data, 1998). The isotopic compositions of the Brandberg granites fall entirely within these values. This overlap alone suggests an important role of mantle-derived material in the Brandberg magma source.

It is difficult to determine from isotopic evidence alone which of the different basic magma types represented locally (e.g. flood basalts in the Goboboseb mountains, parental basalts to the cumulate gabbros from Messum) was involved in the Brandberg magma genesis. One approach is to examine ratios of highly incompatible trace elements together with the isotopic ratios, which distinguish between the LTZ.H and LTZ.L groups. Figure 10 plots the composition of the Brandberg metaluminous granitoids together with representatives of the LTZ.H basalt and LTZ.L basalts from the Etendeka Group in a diagram of εNd and Ta/Yb. The two basalt series define clearly separate trends in the diagram, and the composition of the Brandberg granites plots between the LTZ.H compositions and the field for an upper-crustal granitic basement. Isotopically, the Brandberg magmas, and in particular the least differentiated monzonites, also show a closer affinity to the LTZ.H basalts than to the LTZ.L group, which have much higher Sr initial ratios and more negative εNd values (see Fig. 9). Ewart *et al.* (1998*a*) stated that the LTZ.H suite of the Goboboseb basalts emanated at least in part from the Messum centre, suggesting that the magma source region for the Messum and Brandberg complexes might be very similar.

PETROGENETIC MODELLING

The crustal and mantle components involved in the Brandberg petrogenesis remain ambiguous, especially if evolved and extremely fractionated rocks such as the Amis peralkaline granites are considered. The petrogenetic modelling in this section therefore limits itself to describing the internal evolution of the Brandberg complex. Our goals are to test the hypothesis that the metaluminous granites could have differentiated from a basic parental magma, and to put realistic constraints on the mixing proportions of mantle and crustal material required to explain the Sr and Nd isotopic variations among the Brandberg units. The parental magma is considered to be equivalent to the intermediate Naib valley monzonite, which itself probably had a more basic parent (see previous section). After establishing a model for the differentiation of the metaluminous granites, we then discuss what differences in degree or kind of differentiation are required to explain the origin of the peralkaline suite.

Evolution of the metaluminous suite

The relative order of geochemical differentiation in the metaluminous suite (see Fig. 6) is consistent with the emplacement sequence inferred from field relations, from monzonite to biotite–hornblende granite, followed by biotite leucogranite and finally aplitic dykes. The trachydacite dykes are external to the massif and their position in the emplacement sequence is unknown. Geochemical variations support the hypothesis that the metaluminous suite represents a differentiation series, with the monzonite as an initial magma and the aplites as the final residual melt. However, some degree of mixing or assimilation of more than one source is indicated by the

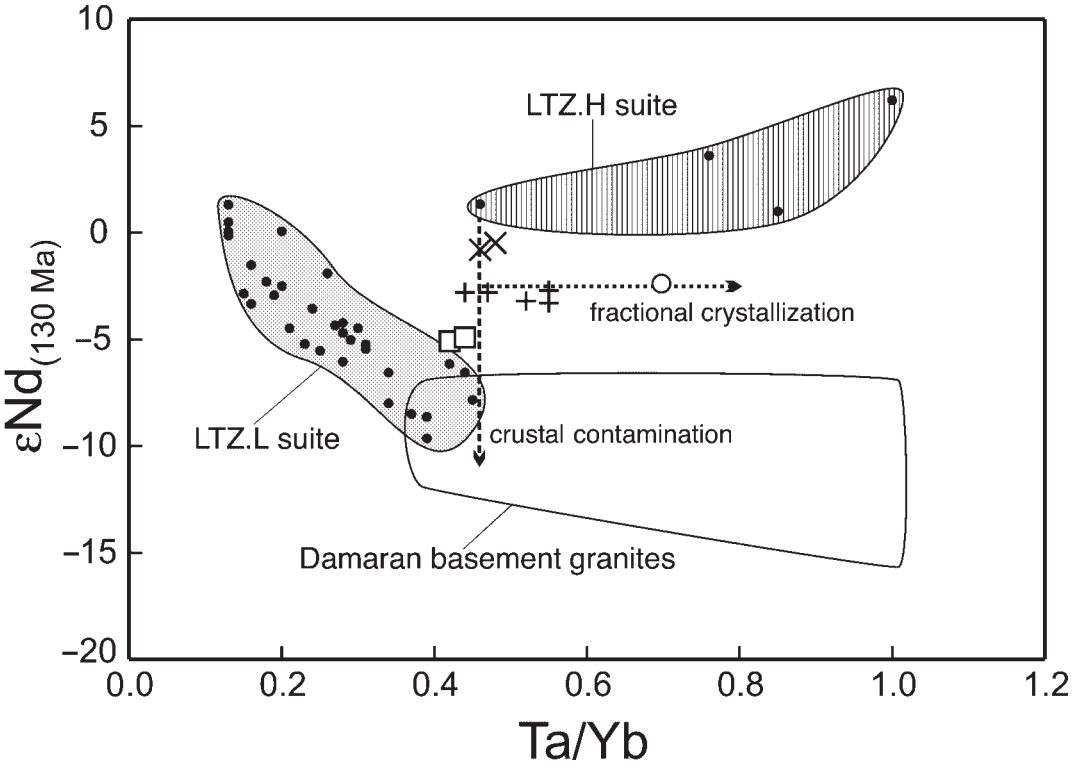

Fig. 10. Ta/Yb vs εNd for metaluminous rocks of the Brandberg complex compared with low-Ti basalts of the Etendeka–Paraná [Paraná data from Garland *et al.* (1995, 1996) and Peate & Hawkesworth (1996)]. The different trend for LTZ.H basalts (Ewart *et al.*, 1998*b*) should be noted. Arrows indicate schematic trends for mixing between an evolved LTZ.H basaltic magma and crust and fractional crystallization as observed within the Brandberg metaluminous suite. Field shows range for leucogranite and Salem granite data from McDermott *et al.* (1996). It should be noted that the Brandberg samples plot off the mixing trend between LZT.L and crustal compositions. Symbols as in Fig. 9.

isotopic data. Whereas the biotite–hornblende granite and biotite leucogranite overlap in initial isotopic ratios and can be strictly comagmatic, the monzonite has distinctly lower initial Sr and higher Nd isotopic ratios than these. The samples from the trachydacite dykes, by contrast, have higher initial Sr and lower Nd ratios.

Mixing and AFC processes

Mixing and AFC calculations were made to test the degree of crustal assimilation vs fractionation required in producing the Brandberg main massif granites from a parental monzonite magma. The starting composition is represented by monzonite sample B21d. The choice of crustal component was made to cover two types of assimilation, i.e. bulk assimilation of crust and mixing of basic parental magma with partial melts of the crust (assuming the monzonite magma to be the heat source for anatexis). The compositions used for bulk assimilation are typical of the dominant rock types in the local crust, S-type Salem granite (McDermott *et al.*, 1996) and greywacke-type metasediments (Ewart *et al.*, 1998*a*). For a typical anatectic melt from metasediments the composition of a leucogranite as given by Garland *et al.* (1995) was applied, with its Sr and Nd isotopic composition adjusted to conform to the Damara metasedimentary basement. Mixing with felsic magmas equivalent to the Etendeka quartz latite units was also tested, using average compositions of Goboboseb quartz latites from Ewart *et al.* (1998*b*).

The crucial factors in AFC modelling are bulk distribution coefficients (D values) for the fractionating assemblage and the ratio of crystallization rate to assimilation rate (r). Individual mineral–melt k_D values (for intermediate compositions) were taken from the literature (references in Table 7) and bulk D was derived from the mode of the fractionating assemblage calculated from a major element mixing model (least-squares) between monzonite and biotite–hornblende granite using mineral compositions analysed by electron microprobe (Tables 1 and 2) and using a $Mag_{41}Usp_{59}$ titanomagnetite composition typical for the Brandberg trachydacites. The least-squares solution indicates a high proportion of plagioclase relative to clinopyroxene and magnetite in the fractionating assemblage. The calculated plagioclase–

clinopyroxene–Ti-magnetite ratios are 0·58:0·22:0·20 [f (mass remaining magma/mass initial magma) = 0·73; ΣR^2 (sum of squares of residuals between actual and calculated starting composition) = 0·38]. This result is consistent with the crystallization sequence predicted by the MELTS thermodynamic model (Ghiorso & Sack, 1995) for a monzonite parental melt [300 MPa, quartz–fayalite–magnetite (QFM) buffer, 1 wt % H_2O], which indicated magnetite as a liquidus phase, a high abundance of plagioclase and a ratio of magnetite to clinopyroxene in the fractionating assemblage of about unity.

The graphical method of Aitcheson & Forrest (1994) was used to estimate the values of (r) and the mass ratio of crustal assimilant to initial magma by intersection of AFC curves. For simplicity, no recharge was assumed. Curves were calculated for Nd and Sr isotopic ratios and a subset of trace elements that are not controlled by accessory minerals. Figure 11 illustrates the results. In the case of a Salem granite and a leucogranite contaminant, most curves intersect at values for r (ratio of assimilation to crystallization rate) of ~0·4–0·8 for the hornblende–biotite granite. The calculated ρ value (mass ratio of assimilant to initial magma) is in the range between 0·2 and 0·3. Less constrained values (i.e. poor intersections) resulted for models using the greywacke composition as the crustal contaminant. The AFC curves calculated for quartz latite as a contaminant fail to yield a consistent solution at r <1, which we consider as a thermal limit for the AFC process.

The same modelling approach was performed to test the degree of crustal assimilation required to derive the trachydacite dykes from a monzonitic parent. A good fit was obtained by mixing between monzonitic magma with ~40% crustal material (Salem granite), matching observed isotopic and trace element compositions.

The deviations between calculated and observed trace element abundances and isotopic ratios for AFC and mixing models are summarized in Table 7. Figure 9 shows AFC curves calculated for the Sr and Nd isotopic data using values of r and ρ derived from the Aitcheson & Forrest (1994) method. The results demonstrate that evolution of the Brandberg metaluminous granites from a monzonitic parental magma can be achieved by a process of fractionation of parental monzonite magma with some 20–40% crustal assimilation.

Differentiation of the metaluminous suite

The variation in composition within the main massif granites (68–72 wt % SiO_2 in biotite–hornblende granite and 76 wt % in biotite leucogranite) is not associated with a shift in isotopic composition; thus a closed-system fractionation model is feasible. Table 8 presents least-squares mixing calculations (major elements) set up to test the hypothesis that fractional crystallization can explain the chemical variation within the metaluminous granites. The modelling was performed in stages to allow for changes in the fractionating assemblage. Mineral compositions used were those measured by electron microprobe except for exsolved Fe–Ti-oxide mineral phases. The mineral proportions from major element mixing calculations were then used to calculate bulk D values and trace element modelling was performed for selected elements using the Rayleigh equation and rhyolite mineral–melt distribution coefficients (k_D values) from the literature. In high-Si rhyolites, accessory mineral fractionation may severely affect certain trace elements, such as Zr and REE. Therefore, modelling was restricted to Rb, Sr and Ba, all of which are dominantly controlled by major mineral phases, i.e. pyroxene–amphibole and feldspar. Fluorine was included as it shows strong enrichments in the metaluminous suite with increasing differentiation and is likewise hosted by major phases.

The results demonstrate that compositional variation between the least-evolved hornblende–biotite granite (sample NU40, 68 wt % SiO_2) and an evolved hornblende–biotite granite (sample NU22, 71 wt % SiO_2) can be explained by ~50% fractional crystallization of an assemblage consisting of feldspar (nominal composition $Ab_{55}An_{10}Or_{35}$), quartz, clinopyroxene (or amphibole) and biotite. A further 20% crystallization of this evolved granite can produce a residual melt equivalent to the biotite leucogranite (sample B8, 76 wt % SiO_2) by removal of a feldspar-dominated assemblage (71% $Ab_{67}An_{13}Or_{20}$, 6% quartz, 23% biotite). The step from this leucogranite (B8) to the most highly evolved metaluminous aplitic dyke-rock (NU25a) requires a change in the fractionating assemblage, with quartz and K-feldspar as the most abundant phases (37% quartz, 54% $Ab_{38}An_5Or_{57}$, 9% biotite), and a relatively low f value of 0·51 is indicated. The trace element modelling is concordant with these results. Table 8 presents f values calculated from the Rayleigh equation for Rb, Sr and Ba (including fluorine), which in most cases agree with the f values indicated by the major element mixing calculations within Δf = 0·1 (abs.).

The peralkaline suite

The peralkaline granites of the Amis complex are the compositionally most variable group of all Brandberg units, as major element and trace element compositions are strongly controlled by mineral segregation and, to some extent, secondary accessory mineral growth. The Nd isotopic data reveal a spread in values among the peralkaline group between εNd of −0·7 and −1·9. The Nd isotopic compositions of the monzonite and the biotite–hornblende granites bracket these values, which

Table 7: Parameters and compositions used for calculation of crust/mantle ratios in Brandberg metaluminous rocks after the method of Aitcheson & Forrest (1994)

Model:	AFC	AFC	AFC	AFC	Mixing			
Parent:	B21d	B21d	B21d	B21d	B21d			
Assimilant:	C_a (a) Salem granite	C_a (b) leuco-granite	C_a (c) Damara greywacke	C_a (d) quartz latite	C_a (a) Salem granite			
Target:	NU40	NU40	NU40	NU40	GO07			
pl:cpx:mag:	58:22:20	58:22:20	58:22:20	58:22:20	—			
	$r = 0{\cdot}6$	$r = 0{\cdot}8$	$r = 0{\cdot}6$	$r = 0{\cdot}9$	$f = 0{\cdot}4$			
	$f = 0{\cdot}9$	$f = 0{\cdot}95$	$f = 0{\cdot}9$	$f = 0{\cdot}95$	—			
	e *and* c *values*					k_D *values*		
						pl	*cpx*	*mag*
$^{87}Sr/^{86}Sr_{(130\,Ma)}$	0·724	0·730	0·730	0·721	0·724			
$\varepsilon Nd_{(130\,Ma)}$	−15·3	−17·1	−10·0	−9·0	−15·3			
Sr	249	124	154	153	249	4·4	0·50	0·01
Rb	171	230	135	157	171	0·30	0·02	0·01
Ba	909	375	608	688	909	0·48	0·10	0·10
La	70	18	26	46	70	0·30	0·52	0·66
Nd	45	30	37	44	45	0·19	1·4	0·93
Y	26	21	40	48	26	0·08	2·7	0·95
Relative deviation								
Δe_m (‰)								
$^{87}Sr/^{86}Sr_{(130\,Ma)}$	−1·8	−2·0	−2·2	1·2	−1·9			
$\varepsilon Nd_{(130\,Ma)}$	0·07	0·07	0·15	−0·01	−0·09			
Δc_m (%)								
Sr	10	0	2	−29	22			
Rb	−5	1	−8	10	4			
Ba	2	−10	−3	6	−3			
La	−9	−23	−18	−8	−13			
Nd	−13	−19	−15	−11	−22			
Y	−3	−7	1	1	−25			

Isotopic ratios (*e*) and trace element concentrations (*c*) of assimilants are given. Parent and target compositions are given in Tables 4 and 6. Relative deviation between observed and calculated values for AFC and mixing calculations using B21d as parental magma and different crustal contaminants is shown. C_a, concentration and isotopic composition of assimilants: C_a (a), Salem granite from McDermott *et al.* (1996); C_a (b), Langtang leucogranite after Garland *et al.* (1995) using average isotopic ratios for Damara leucogranites from McDermott *et al.* (1996); C_a (c), greywacke from Ewart *et al.* (1998*a*); C_a (d), average quartz latite from Ewart *et al.* (1998*b*). Concentrations are in ppm, isotopic ratios recalculated for 130 Ma. Mineral–melt distribution coefficients for clinopyroxene (k_D cpx), plagioclase (k_D pl) and magnetite (k_D mag) for intermediate compositions from Ewart & Griffin (1994) and Bacon & Druitt (1988). *r*, ratio of assimilation/crystallization; *f*, ratio of mass melt remaining/mass original melt. Δe_m, relative deviation between modelled and observed isotopic ratios; $\Delta e_m = [(e_{modelled}/e_{observed}) - 1] \times 1000$. Δc_m, relative deviation between modelled and observed trace element composition; $\Delta c_m = [(c_{modelled}/c_{observed}) - 1] \times 100$.

allows us to envisage a parental magma for the peralkaline melt from the Brandberg metaluminous suite. On the grounds of mass balance calculations, it can be shown that fractional crystallization of phases with (Na + K)/Al <1 (in particular calcic plagioclase) from a metaluminous parent can produce a peralkaline residual melt (e.g. Harris, 1983).

There is unequivocal evidence for the highly fractionated nature of the peralkaline granites: high Rb and F, and extremely low Sr, Ba and Eu/Eu*. According to these indices the degree of fractionation in the peralkaline suite exceeds that of the most evolved metaluminous leucogranite. In the metaluminous suite concentrations of HFSE, notably Zr, Nb and REE, remain constant or

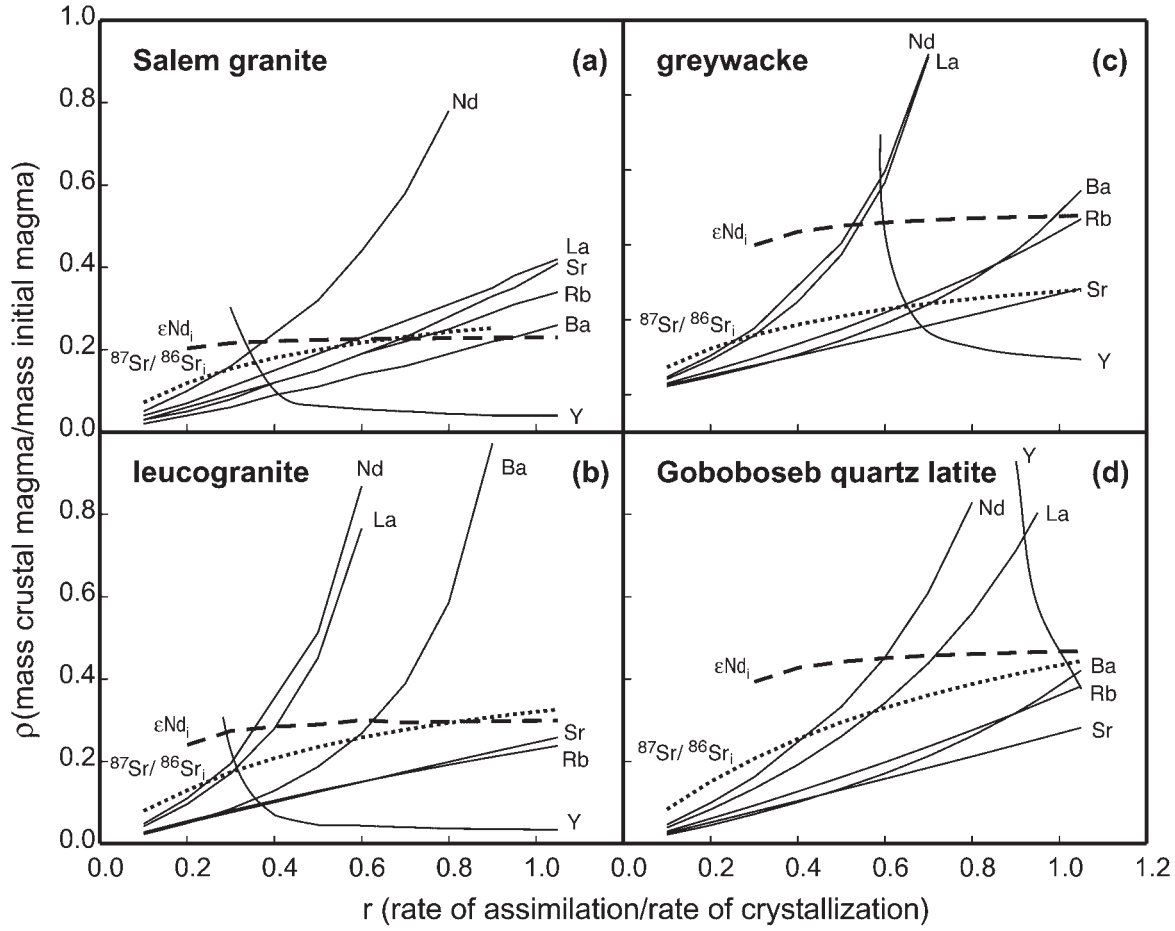

Fig. 11. Calculated AFC mixing curves for selected trace elements (thin continuous lines) and Nd–Sr isotope ratios (thick broken lines) based on equations of Aitcheson & Forrest (1994). Values for monzonite (parent), biotite–hornblende granite (contaminated magma), various contaminants [Salem granite (a), leucogranite (b), greywacke (c) and quartz latite (d)] and bulk D calculated from k_D values are given in Table 7. Isotope curves, which do not require element concentrations in the contaminated magma, converge at r values between 0·6 and 0·8 for granitic contaminants (i.e. crustally derived partial melts) in (a) and (b). Models (c) and (d) fail to yield consistent solutions.

fall with fractionation from biotite–hornblende granite to biotite granite. In the Amis peralkaline rocks, by contrast, these elements can reach high levels in a comparable narrow range of SiO_2. Microprobe analyses of melt inclusions hosted in quartz give direct evidence that the high HFSE (and Rb) contents can be attributed to enrichment in a residual melt phase (Table 5).

In part, the enrichment levels of some of these elements are higher than Rayleigh fractionation could generate even assuming ideally incompatible behaviour. Post-magmatic processes such as element transport by hydrothermal fluids could account for these enrichments, although the granites in question largely preserved magmatic textures and pervasive post-emplacement metasomatism can be ruled out. Trace elements that are sensitive to hydrothermal effects, such as Y/Ho and Zr/Hf (Bau & Dulski, 1995; Bau, 1996) are generally only moderately displaced from magmatic values (Y/Ho = 24–34 and Zr/Hf = 26–46 compared with the range in the peralkaline granites of Y/Ho = 21 and Zr/Hf in zircon cores from peralkaline granites of ~30).

However, mineral overgrowth textures, interstitial REE-bearing fluorite and bastnaesite, and zonations in accessory minerals such as pyrochlore and zircon indicate late-stage, probably fluid-controlled overprint. For example, anomalous REE patterns displaying the lanthanide tetrad effect and zoned zircon crystals from aegirine–albite granites with low Zr/Hf rim compositions (Zr/Hf ~ 10) might reveal a change from primary magmatic to fluid-dominated conditions.

We cannot model the element enrichments, because of the lack of data on element partitioning and accessory mineral solubilities in a volatile-rich peralkaline magma. Experiments by Watson (1979) and Keppler (1993), among others, demonstrate that peralkaline and F-rich melts can dissolve high quantities of HFSE by virtue of

Table 8: Results of least-squares mixing calculations to test a fractional crystallization model for metaluminous units of the Brandberg complex

Model 1: primitive to evolved biotite–hornblende granite
SiO_2 68–72 wt % (ΣR^2 0·07)

				k_D value						
	parent NU40 (ppm)	daughter NU22 (ppm)	pl 35%	cpx 6%	Fe–Ti oxide 1%	bt 17%	qtz 21%	kfs 20%	*D*	*F* 0·47 *f* (calc)
Rb	186	279	0·03	0·03	—	2·46	0	0·11	0·46	0·56
Sr	147	96	4·4	0·06	—	0·25	0	2·11	2·02	0·66
Ba	1017	739	1·0	0·03	—	6·4	0	2·7	1·99	0·72
F	1350	2400	0	0	—	1·59	0	0	0·27	0·45

Model 2: evolved biotite–hornblende granite to primitive biotite leucogranite
SiO_2 72–76 wt % (ΣR^2 0·14)

				k_D value						
	parent NU22 (ppm)	daughter B8 (ppm)	pl 54%	kfs 17%	qtz 6%	bt 23%			*D*	*F* 0·78 *f* (calc)
Rb	279	329	0·01	0·11	0	2·46			0·59	0·67
Sr	96	37	12·2	2·11	0	0·25			7·0	0·85
Ba	739	210	1·8	20·9	0	6·4			6·0	0·78
F	2400	2300	0	0	0	1·59			0·37	1·07

Model 3: primitive biotite leucogranite–evolved biotite leucogranite
SiO_2 76–77 wt % (ΣR^2 0·01)

				k_D value						
	parent B8 (ppm)	daughter NU25a (ppm)	pl 17%	kfs 37%	qtz 37%	bt 9%			*D*	*F* 0·51 *f* (calc)
Rb	329	568	0·01	0·11	0	2·46			0·26	0·48
Sr	37	10	12·2	2·11	0	0·25			2·88	0·50
Ba	210	15	1·8	20·9	0	6·4			8·62	0·71
F	2300	3750	0	0	0	1·59			0·14	0·57

Minerals: cpx, clinopyroxene; pl, plagioclase; kfs, K-feldspar; bt, biotite; qtz, quartz; Fe–Ti, ilmenite. Mineral compositions used: qtz stoichiometric, Fe–Ti ilmenite from Deer *et al.* (1992); others from microprobe analysis of the Brandberg rocks. Plag from Table 1, AM71 core; amph from Table 3, NU40; ksp from Table 1, AM71 rim; bt from Table 3, NU22. k_D values for low-Si (model 1) and high-Si rhyolitic compositions (models 2 and 3) from Ewart & Griffin (1994), Icenhower & London (1995) and Streck & Grunder (1997). *D*, bulk mineral–melt distribution coefficient.

depolymerization of silicate melt structure and formation of alkali and fluoro-complexes, and we suggest that this type of process is the prevailing mechanism for the element enrichments in the Amis granites. The magmatic and post-magmatic history of the Amis rocks makes an unequivocal identification of the parental magma impossible, but the close temporal and spatial relation between metaluminous and peralkaline magma types

favours a common basaltic source with some addition of crustal material for both.

No peralkaline rhyolites have been described within the Etendeka volcanic succession, but comendites are present in the Paresis complex (Siedner, 1968). However, there are numerous examples in the literature of similar HFSE enrichments in Si-oversaturated peralkaline and unequivocally magmatic rocks. For example, Mungall & Martin (1995, 1996) studied volcanic glasses and melt inclusions in peralkaline rhyodacites (pantellerites) from Terceira island in the Azores, and reported values of Zr (3000 ppm), Ce (300 ppm) Nb (700 ppm) and Y (200 ppm). These are of the same order as the Amis arfvedsonite granites and clearly represent magmatic concentrations. Like the Amis rocks, the Terceira pantellerites are rich in F (2500–3000 ppm). As a local example for a basalt-derived peralkaline residual liquid, Ewart *et al.* (1998*a*) noted that LTZ.H melts from the Goboboseb mountains evolve towards Si-undersaturated peralkaline and Zr-enriched composition by fractionation while ponding close to the surface. Fractionation of an LTZ.H basalt at depth might result in qtz-normative compositions for the remaining melt.

IMPLICATIONS FOR REGIONAL SILICIC MAGMATISM IN THE ETENDEKA PROVINCE

A number of observations suggest that emplacement of the Brandberg magmas and eruption of Etendeka Group felsic volcanics (Awahab Formation quartz latites) are related to the same igneous event:

(1) close field association between the Brandberg complex and quartz latites that are extensively exposed in the Goboboseb mountains some 10 km SW of the Brandberg;

(2) indistinguishable $^{40}Ar/^{39}Ar$ ages (132 ± 1 Ma);

(3) similar bulk composition and mineralogy indicative of high-temperature, dry granitic magmas;

(4) large magma volumes: $\geq 8600\ km^3$ for the quartz latites (Ewart *et al.*, 1998*b*) and at least $1100\ km^3$ for the Brandberg (minimum estimate for a cylindrical intrusion 2·5 km thick, i.e. the topographic relief).

The Brandberg granites clearly represent a significant proportion of felsic magmas in the Etendeka–Paraná province as a whole, and new constraints on the Brandberg magma genesis derived from this study are useful for understanding the evolution of anorogenic silicic magmatism in general. It was shown earlier that the Brandberg units cannot be correlated with the felsic volcanics from the Etendeka Group in terms of composition and it is important to inquire whether they have different sources or, if both represent hybrid magmas, whether they formed from different proportions of the same components.

Existing petrogenetic models for the felsic magmatism in the Etendeka–Paraná province cover the full range from crustal melting to differentiation from basalt including AFC scenarios. Garland *et al.* (1995) suggested that the high- and low-Ti felsic units in the Paraná province are derived from the respective high- and low-Ti basaltic suites, and that the latter suite had experienced a considerable degree of crustal contamination. Harris & Milner (1997) favoured a dominantly crustal origin for the Etendeka quartz latites based on oxygen isotope compositions, and Ewart *et al.* (1998*b*) presented a petrogenetic model for the quartz latites, which concluded that the magmas are hybrid, having incorporated roughly equal proportions of low-Ti basaltic melt and melts of the crust.

A useful and simple way to compare the degree of mantle vs crustal involvement in granitic magmas based on Nd isotope data was developed by DePaolo *et al.* (1992), and applied to the Tertiary magmatism in the Basin and Range Province of southwestern North America. The Neodymium Crustal Index (NCI) is a mass-balance expression for two-component mixing, which gives the proportion of crustal Nd in a hybrid rock. Two-component mixing may be an oversimplification of the processes involved in forming the silicic magmas on the Namibian margin but the foregoing discussions and simple trajectory of samples on an Sr–Nd isotope plot (Fig. 9) suggest that it is a reasonable approximation.

As the Etendeka felsic volcanics formed in the same region of the Damara Belt at the same time, it is justified to assume, as a first approach, that the same crustal and mantle components were involved. We have already discussed the potential components in the mantle and crust, and the following calculations of the NCI values are based on the assumption that the crustal component is derived from the dominant basement rocks in the Damara Belt (metasediments and crustal granites, hereafter called 'Damara crust'). We applied the method of DePaolo *et al.* [1992, equations (3) and (4)] to estimate an average Nd isotopic composition of the Damara crust from Nd model ages (T_{DM}). Results are shown in Table 9. The T_{DM} values for metasediments calculated from data of McDermott & Hawkesworth (1990) define two ranges, 1·4–1·6 Ga and 1·8–2·0 Ga [see also Harris *et al.* (1987)], the latter corresponding to metasediments lowest in the Damara section (Khan and Etusis Formations). The T_{DM} ages from crustal Damara granites overlap both ranges. The NCI calculations therefore use two values for εNd_{crust} (-7 and -13) corresponding to T_{DM} ages of 1·5 and 1·9 Ga, respectively.

For the mantle component we assume two compositions, one reflecting a more depleted mantle [$\varepsilon Nd = +6$, the maximum value from the Etendeka LTZ.H basalts from Ewart *et al.* (1998*a*)] and one reflecting a

Table 9: NCI values for metaluminous rocks of the Brandberg complex using equations of DePaolo et al. (1992)

Brandberg unit	Crustal type[1]	T_{DM} (Ga)	εNd (rock)	$f^*_{Sm/Nd}$ (T_{DM})	εNd (T_{DM})	εNd(CC)	NCI εMC = 0	NCI εMC = +6
hbl–bt granite	Nama/Kuiseb	1·5	−3	−0·370	5·7	−7·0	0·43	0·69
hbl–bt granite	Khan	1·9	−3	−0·402	5·0	−12·9	0·23	0·48
monzonite	Nama/Kuiseb	1·5	−1	−0·370	5·7	−7·0	0·14	0·54
monzonite	Khan	1·9	−1	−0·402	5·0	−12·9	0·08	0·37
trachydacite	Nama/Kuiseb	1·5	−5	−0·370	5·7	−7·0	0·72	0·85
trachydacite	Khan	1·9	−5	−0·402	5·0	−12·9	0·39	0·58

[1]Crustal types: Nama/Kuiseb, upper Damara metasediments; Khan, lower Damara metasediments; data from McDermott & Hawkesworth (1990) and McDermott *et al.* (1996). Neodymium Crustal Index defined as NCI = $[\varepsilon Nd_{(rock)} - \varepsilon Nd_{(MC)}]/[\varepsilon Nd_{(CC)} - \varepsilon Nd_{(MC)}]$, where MC and CC denotes mantle and crustal component, respectively.

bulk-Earth composition similar to the present Tristan plume (εNd = 0).

The results of the NCI calculations (Table 9) indicate that the proportion of crustal Nd in the most primitive units of the Brandberg (monzonite) is between 0·08 and 0·14 assuming the 'plume-type' mantle and between 0·37 and 0·54 assuming the depleted mantle component. The corresponding NCI values for the main massif granite are 0·23–0·43 for plume mantle and 0·48–0·69 for depleted mantle, respectively. It should be noted that the difference in crustal proportion between monzonite and main granite is ∼20%, which agrees with the estimate of crustal assimilation derived from the AFC modelling in the section on petrogenetic modelling.

The Awahab quartz latites yield NCI values of 0·62–1 for the plume-type mantle composition and 0·74–1 for depleted mantle. Thus, according to this approach, an origin by pure crustal melting cannot be ruled out for the quartz latites (NCI = 1), this condition being met for an average crustal component with εNd values of −7.

These NCI values represent the mass proportions of crustal Nd in the rocks. As the whole-rock Nd concentrations in Etendeka flood basalts (mantle component) and Damara basement overlap (30–50 ppm Nd), we can interpret the NCI values as estimates of the total crustal mass fractions and then compare them with the mixing proportions of Harris (1995) based on O-isotope ratios. Harris (1995) suggested that the mass fraction of crustal material in the Brandberg granite was 0·38, which agrees with our NCI solutions assuming a plume-type mantle component with εNd values of zero. Harris & Milner (1997) suggested that the quartz latites are crustally derived, with no indication of a mantle source based on the O-isotope values. This is also in rough agreement with the NCI calculations, which yielded NCI values close to unity.

In summary, the geological, geochronological and modelling evidence supports that hypothesis that the Brandberg granites and regional felsic volcanic rocks of the Etendeka Group could be derived from similar sources but with different proportions. Figure 9 shows, however, that the AFC curves of the Brandberg samples do not coincide with those of the volcanic rocks even when assuming the same end-member compositions. Apart from end-member composition, the controlling parameters of the AFC curves are the mineral–melt distribution coefficients (k_D values) and the ratio of assimilation to crystallization rates (r values). Bulk D values depend on phase proportions in the fractionating assemblage, whereas the r value is mainly influenced by the temperature difference between magma and assimilant. Using the same end-member compositions for both the Brandberg and flood basalt–rhyolite arrays, the AFC solution for the Brandberg data requires higher bulk D values for Sr and lower r values than the solution for the flood basalt–rhyolite data array. Both of these conditions can be met by assuming that AFC processes operated at different depths, shallower for the Brandberg and deeper for the flood basalt magmas. The phase assemblage crystallizing from basaltic melt at lower pressure has a higher plagioclase/clinopyroxene ratio than at higher pressure, and therefore a higher bulk D value for Sr. Furthermore, if the AFC process occurs at relatively shallow levels in the crust this will impose a low assimilation/crystallization rate (r value) because the wallrocks will be relatively cool, crystallization more rapid and assimilation less effective. Therefore, one factor that could explain the difference between the Brandberg and the Etendeka–Paraná AFC trends is the depth of magma evolution.

CONCLUSIONS

The Cretaceous Brandberg intrusive complex in Namibia is made up dominantly of metaluminous hornblende–biotite granite (main granite), which includes local schlieren and dykes of biotite leucogranite. Other components of the Brandberg complex are a pyroxene–hornblende monzonite (Naib valley monzonite), which is intruded by apophyses of the main granite and therefore older; a body of peralkaline arfvedsonite–aegirine granites that intrudes the main granite at the SW margin (Amis peralkaline complex); and a series of trachydacite dykes that cut the country rocks on the north margin of the main massif.

This geochronological, geochemical and radiogenic isotopic study of the igneous components of the Brandberg has concentrated on a petrogenetic model. The following main constraints on the origin and development of the complex have been developed:

(1) the granites of the main massif and the peralkaline granites have indistinguishable ^{40}Ar–^{39}Ar ages between 132·5 and 130·5 Ma. Thus, the intrusion of the Brandberg granites is coeval with the peak volcanic activity in the Etendeka–Paraná igneous province.

(2) The metaluminous main granite formed from a relatively hot (>850°C minimum temperatures from zircon solubility and pyroxene thermometry) and dry magma (<3 wt % H_2O is required for concordant monazite and zircon thermometry) in a near-surface intrusion.

(3) Sr- and Nd-isotopic composition of the metaluminous and peralkaline Brandberg granites rules out derivation from crustal sources alone. The data suggest that the granites evolved by fractionation of a basaltic source similar to the LTZ.H series, which crop out in the nearby Goboboseb area. However, the isotopic data and elevated large ion lithophile element concentrations require assimilation of crustal material. AFC modelling suggests a mass proportion of crustal material similar to the Damara granites or leucogranitic partial melts derived from local metasediments in the range of 20–40%.

(4) The Brandberg granites show much less crustal influence than the contemporary felsic volcanics (quartz latites) of the Etendeka group and do not plot along the same crust–mantle AFC curves.

(5) Fractional crystallization of plagioclase, clinopyroxene–hornblende, alkali feldspar and Fe–Ti oxides can explain the compositional variety within the metaluminous group, from monzonite (62 wt % SiO_2) to biotite leucogranite (73 wt % SiO_2).

(6) The peralkaline granites (72–77 wt % SiO_2) intrude the granite of the main massif and are therefore younger. Post-magmatic alteration of the peralkaline granites is locally indicated by quartz–haematite overgrowths, but the distinctive mineralogical and geochemical characters of the peralkaline granites are interpreted as primary features because they are found in all textural varieties of the complex, from thin aplite dykes to homogeneous granite to coarse pegmatites. Unequivocal proof of a magmatic origin for the typical chemical features (high F, Zr, Y and REE) is given by the presence of melt inclusions with these characteristics in quartz from arfvedsonite granite pegmatite. Field and age relations and Nd-isotopic composition suggest a common origin for the metaluminous and peralkaline suites.

ACKNOWLEDGEMENTS

The authors wish to thank H. Gerstenberger, G. Haase, C. Schulz and R. Romer, GeoForschungsZentrum Potsdam, for carefully carrying out Sr- and Nd-isotopic analyses. K. Menge and H. Klappert are thanked for preparation of mineral separates and performing the Ar measurements at the BGR, Hannover. P. Dulski, GeoForschungsZentrum Potsdam, is thanked for ICP-MS analyses. We also thank R. Thomas for providing unpublished data on melt inclusions of the Amis peralkaline granites. M. Stock, R. A. Balooney and M. Zimmermann contributed in field mapping and electron microprobe analysis. Help and advice in electron microprobe work from R. Borchardt and XRF analyses from M. Grünhäuser, University of Giessen, are greatly appreciated. The Geological Survey of Namibia, especially G. Schneider and S. Milner, is thanked for co-operating during field studies. This study was supported by DFG Grant Em23/10 to R.E. This contribution benefited greatly from critical comments by Chris Harris, Simon Milner and an anonymous reviewer on an earlier version of the manuscript. Marjorie Wilson is thanked for editorial advice.

REFERENCES

Aitcheson, S. J. & Forrest, A. H. (1994). Quantification of crustal contamination in open magmatic systems. *Journal of Petrology* **35**, 461–488.

Anders, E. & Grevesse, N. (1989). Abundances of the elements: meteoritic and solar. *Geochimica et Cosmochimica Acta* **53**, 197–214.

Anderson, J. L. & Smith, D. R. (1995). The effects of temperature and fO_2 on the Al-in-hornblende barometer. *American Mineralogist* **80**, 549–559.

Armstrong, R. A., McDougall, I. & Watkins, R. T. (1997). U/Pb zircon ages of Damaraland complexes, Namibia. *EOS Transactions, American Geophysical Union* **78**, 742.

Bacon, C. R. & Druitt, T. H. (1988). Compositional evolution of the zoned calcalkaline magma chamber of Mount Mazama, Crater Lake, Oregon. *Contributions to Mineralogy and Petrology* **98**, 224–256.

Bau, M. (1996). Controls on the fractionation of isovalent trace elements in magmatic and aqueous systems; evidence from Y/Ho, Zr/Hf, and lanthanide tetrad effect. *Contributions to Mineralogy and Petrology* **123**, 323–333.

Bau, M. & Dulski, P. (1995). Comparative study of yttrium and rare-earth element behaviours in fluorine-rich hydrothermal systems. *Contributions to Mineralogy and Petrology* **123**, 323–333.

Bowden, P., Kinnaird, J. A., Diehl, M. & Pirajno, F. (1990). Anorogenic granite evolution in Namibia; a fluid contribution. *Geological Journal* **25**, 381–390.

Christiansen, E. H. & Lee, D. E. (1986). Fluorine and chlorine in granitoids from the Basin and Range Province, Western United States. *Economic Geology* **81**, 1484–1494.

Clemens, J. D., Holloway, J. R. & White, A. J. R. (1986). Origin of A-type granite: experimental constraints. *American Mineralogist* **71**, 317–324.

Cloos, H. & Chuboda, K. (1931). Der Brandberg. Bau, Bildung und Gestalt der jungen Plutone in Südwestafrika. *Neues Jahrbuch für Mineralogie, Geologie und Paläontologie Beilage* **66B**, 1–130.

Collins, W. J., Beams, S. D., White, A. J. R. & Chappell, B. W. (1982). Nature and origin of A-type granites with particular reference to southeastern Australia. *Contributions to Mineralogy and Petrology* **80**, 189–200.

Creaser, R. A., Price, R. C. & Wormald, R. J. (1991). A-type granites: assessment of a residual-source model. *Geology* **19**, 163–166.

Deer, W. A., Howie, R. A. & Zussman, J. (1992). *An Introduction to the Rock-forming Minerals*. Harlow, UK: Longman.

DePaolo, D. J., Perry, F. V. & Baldridge, W. S. (1992). Crustal versus mantle sources of granitic magmas: a two-parameter model based on Nd isotopic studies. *Transactions of the Royal Society of Edinburgh, Earth Sciences* **83**, 439–446.

Diehl, M. (1990). Geology, mineralogy, geochemistry and hydrothermal alteration of the Brandberg alkaline complex, Namibia. *Geological Survey of Namibia Memoir* **10**, 1–55.

Droop, G. T. R. (1987). A general equation for estimating Fe^{3+} concentrations in ferromagnesian silicates and oxides from microprobe analyses, using stoichiometric criteria. *Mineralogical Magazine* **51**, 431–435.

Eby, N. (1990). The A-type granitoids: a review of their occurrence and chemical characteristics and speculations on their petrogenesis. *Lithos* **26**, 115–134.

Eby, N. (1992). Chemical subdivision of the A-type granitoids: petrogenetic and tectonic implications. *Geology* **20**, 641–644.

Erlank, A. J., Marsh, J. S., Duncan, A. R., Miller, R. McG., Hawkesworth, C. J., Betton, P. J. & Rex, D. C. (1984). Geochemistry and petrogenesis of the Etendeka volcanic rocks from SWA/Namibia. *Special Publication of the Geological Society of South Africa* **13**, 195–246.

Ewart, A. & Griffin, W. L. (1994). Application of proton-microprobe data to trace-element partitioning in volcanic rocks. *Chemical Geology* **117**, 251–284.

Ewart, A., Milner, S. C., Armstrong, R. A. & Duncan, A. R. (1998*a*). Etendeka volcanism of the Goboboseb Mountains and Messum Igneous Complex, Namibia. Part I: Geochemical evidence of early Cretaceous Tristan Plume melts and the role of crustal contamination in the Paraná–Etendeka CFB. *Journal of Petrology* **39**, 191–225.

Ewart, A., Milner, S. C., Armstrong, R. A. & Duncan, A. R. (1998*b*). Etendeka volcanism of the Goboboseb Mountains and Messum Igneous Complex, Namibia. Part II: voluminous quartz latite volcanism of the Awahab magma system. *Journal of Petrology* **39**, 227–253.

Faryad, S. W. & Henjes-Kunst, F. (1997). Petrological and K–Ar and ^{40}Ar–^{39}Ar age constraints for the tectonothermal evolution of the high-pressure Meliata unit, Western Carpathians (Slovakia). *Tectonophysics* **280**, 141–156.

Garland, F., Hawkesworth, C. J. & Mantovani, M. S. M. (1995). Description and petrogenesis of the Paraná Rhyolites, Southern Brazil. *Journal of Petrology* **36**, 1193–1227.

Garland, F., Turner, S. & Hawkesworth, C. J. (1996). Shifts in the source of the Paraná basalts through time. *Lithos* **37**, 323–343.

Ghiorso, M. S. & Sack, R. O. (1995). Chemical mass transfer in magmatic processes; IV. A revised and internally consistent thermodynamic model for the interpolation and extrapolation of liquid–solid equilibria in magmatic systems at elevated temperatures and pressures. *Contributions to Mineralogy and Petrology* **119**, 197–212.

Gladczenko, T. P., Hinz, K., Eldholm, O., Meyer, H., Neben, S. & Skogseid, J. (1997). South Atlantic volcanic margins. *Journal of the Geological Society, London* **154**, 465–470.

Govindaraju, K., Potts, P. J., Webb, P. C. & Watson, J. S. (1994). Report on Whin Sill Dolerite WSE from England and Pitscurrie Microgabbro PM-S from Scotland: assessment by one hundred and four international laboratories. *Geostandards Newsletter* **18**, 211–300.

Haack, U., Hoefs, J. & Gohn, E. (1983). Genesis of Damaran granites in the light of Rb/Sr and $\delta^{18}O$ data. In: Martin, H. & Eder, F. W. (eds) *Intracontinental Fold Belts*. Berlin: Springer, pp. 847–872.

Harris, C. (1983). The petrology of lavas and associated plutonic inclusions of Ascension Island. *Journal of Petrology* **24**, 424–470.

Harris, C. (1995). Oxygen isotope geochemistry of the Mesozoic anorogenic complexes of Damaraland, Northwest Namibia: evidence for crustal contamination and its effect on silica saturation. *Contributions to Mineralogy and Petrology* **122**, 308–321.

Harris, C. & Milner, S. (1997). Crustal origin for the Paraná rhyolites: discussion of 'Description and petrogenesis of the Paraná rhyolites, Southern Brazil' by Garland *et al.* (1995). *Journal of Petrology* **38**, 299–302.

Harris, C. & Rickard, R. S. (1987). Rare-earth-rich eudialyte and dalyite from a peralkaline granite dyke at Straumsvola, Dronning Maud Land, Antarctica. *Canadian Mineralogist* **25**, 755–762.

Harris, N. B. W., Hawkesworth, C. J., van Calsteren, P. & McDermott, F. (1987). Evolution of continental crust in Southern Africa. *Earth and Planetary Science Letters* **83**, 85–93.

Hawkesworth, C. J., Kramers, J. D. & Miller, R. M. (1981). Old model Nd ages in Namibian Pan-African rocks. *Nature* **289**, 278–282.

Hess, J. C. & Lippolt, H. J. (1994). Compilation of K–Ar measurements on HD-B1 standard biotite 1994 status report. In: Odin, G. S. (ed.) *Bulletin of Liaison and Informations. IGCP Project 196, Calibration of the Phanerozoic Time Scale 12*. International Geological Correlation Programme, pp. 19–23.

Hodgson, F. D. I. (1972). The geology of the Brandberg–Aba Huab area, South West Africa. Ph.D. Thesis, University of the Orange Free State, Bloemfontein.

Hodgson, F. D. I. (1973). Petrography of the Brandberg intrusion, South West Africa. *Special Publication of the Geological Society of South Africa* **3**, 339–342.

Icenhower, J. & London, D. (1995). An experimental study of element partitioning among biotite, muscovite, and coexisting peraluminous silicic melt at 200 MPa H_2O. *American Mineralogist* **80**, 1229–1251.

Jung, S., Mezger, K. & Hoernes, S. (1998). Petrology and geochemistry of syn- to post-collisional metaluminous A-type granites; a major and trace element and Nd–Sr–Pb–O-isotope study from the Proterozoic Damara Belt, Namibia. *Lithos* **45**, 147–175.

Keppler, H. (1993). Influence of fluorine on the enrichment of high field strength trace elements in granitic rocks. *Contributions to Mineralogy and Petrology* **114**, 479–488.

King, P. L., White, A. J. R., Chappell, B. W. & Allen, C. M. (1997). Characterization and origin of aluminous A-type granites from the Lachlan Fold Belt, Southeastern Australia. *Journal of Petrology* **38**, 371–391.

Korn, H. & Martin, H. (1954). The Messum igneous complex in South-West Africa. *Transactions of the Geological Society of South Africa* **57**, 83–124.

LeBas, M. J., LeMaitre, R. W., Streckeisen, A. & Zanettin, B. (1986). A chemical classification of volcanic rocks based on the total alkali–silica diagram. *Journal of Petrology* **27**, 745–750.

le Roex, A. P. & Lanyon, R. (1998). Isotope and trace element geochemistry of Cretaceous Damaraland lamprophyres and carbonatites, northwestern Namibia; evidence for plume–lithosphere interactions. *Journal of Petrology* **39**, 1117–1146.

Lindsley, D. H. (1983). Pyroxene thermometry. *American Mineralogist* **68**, 477–493.

McDermott, F. & Hawkesworth, C. J. (1990). Intracrustal recycling and upper-crustal evolution; a case study from the Pan-African Damara mobile belt, central Namibia. *Chemical Geology* **83**, 263–280.

McDermott, F., Harris, N. B. W. & Hawkesworth, C. J. (1996). Geochemical constraints on crustal anatexis: a case study from the Pan-African granitoids of Namibia. *Contributions to Mineralogy and Petrology* **123**, 406–423.

Miller, R. McG. (1983). The Pan-African Damara orogen of South West Africa/Namibia. *Special Publication of the Geological Society of South Africa* **11**, 431–515.

Milner, S. C. (1988). The geology and geochemistry of the Etendeka Formation quartz latites, Namibia. Ph.D. Thesis, University of Cape Town.

Milner, S. C. & Duncan, A. R. (1987). Geochemical characterisation of quartz latite units in the Etendeka Formation. *Communications of the Geological Survey of South West Africa/Namibia* **3**, 83–90.

Milner, S. C. & le Roex, A. P. (1996). Isotope characteristics of the Okenyenya igneous complex, Northwestern Namibia: constraints on the composition of the early Tristan plume and the origin of the EM 1 mantle component. *Earth and Planetary Science Letters* **141**, 277–291.

Milner, S. C., Duncan, A. R., Whittingham, A. M. & Ewart, A. (1995*a*). Trans-Atlantic correlation of eruptive sequences and individual silicic volcanic units within the Paraná–Etendeka igneous province. *Journal of Volcanology and Geothermal Research* **69**, 137–157.

Milner, S. C., le Roex, A. P. & O'Connor, J. M. (1995*b*). Age of Mesozoic igneous rocks in northwestern Namibia, and their relationship to continental breakup. *Journal of the Geological Society, London* **152**, 97–104.

Montel, J. M. (1993). A model for monazite melt equilibrium and applications to the generation of granitic magmas. *Chemical Geology* **110**, 127–146.

Mungall, J. E. & Martin, R. F. (1995). Petrogenesis of basalt–comendite and basalt–pantellerite suites, Terceira, Azores, and some implications for the origin of ocean-island rhyolites. *Contributions to Mineralogy and Petrology* **119**, 43–55.

Mungall, J. E. & Martin, R. F. (1996). Extreme differentiation of peralkaline rhyolite, Terceira, Azores: a modern analogue of Strange Lake, Labrador? *Canadian Mineralogist* **34**, 769–777.

O'Connor, J. M. & le Roex, A. P. (1992). South Atlantic hot spot–plume systems; 1. Distribution of volcanism in time and space. *Earth and Planetary Science Letters* **113**, 343–364.

Odin, G. S. (1993). Notes on the intercalibration of reference materials; K–Ar dating. In: Odin, G. S. (ed.) *Bulletin of Liaison and Informations. IGCP Project 196, Calibration of the Phanerozoic Time Scale 12*. International Geological Correlation Programme, p. 18.

Patiño Douce, A. E. (1997). Generation of metaluminous A-type granites by lower pressure melting of calc-alkaline granitoids. *Geology* **25**, 743–746.

Peate, D. W. (1997). The Paraná–Etendeka Province. *Geophysical Monograph, American Geophysical Union* **100**, 217–246.

Peate, D. W. & Hawkesworth, C. J. (1996). Lithospheric to asthenospheric transition in low-Ti flood basalts from Southern Paraná, Brazil. *Chemical Geology* **127**, 1–24.

Peate, D. W., Hawkesworth, C. J. & Mantovani, M. S. M. (1992). Chemical stratigraphy of the Paraná Lavas (S. America): classification of magma types and their spatial distribution. *Bulletin of Volcanology* **55**, 119–139.

Peate, D. W., Hawkesworth, C. J., Mantovani, M. S., Rogers, N. W. & Turner, S. P. (1999). Petrogenesis and stratigraphy of the high-Ti/Y Urubici magma type in the Paraná flood basalt province and implications for the nature of 'Dupal'-type mantle in the South Atlantic region. *Journal of Petrology* **40**, 451–473.

Porada, H. (1979). The Damara–Ribeira Orogen of the Pan-African–Brasiliano cycle in Namibia (SW Africa) and Brazil as interpreted in terms of continental collision. *Tectonophysics* **57**, 237–256.

Porada, H. (1989). Pan-African rifting and orogenesis in southern Equatorial Africa and eastern Brazil. *Precambrian Research* **44**, 103–136.

Pouchou, J. L. & Pichoir, F. (1984). An new model of quantitative X-ray microanalysis—part 1: Application to the analysis of homogeneous samples. *La Recherche Aérospatiale* **3**, 13–38.

Rabinowitz, P. D. & LaBrecque, J. L. (1979). The Mesozoic South Atlantic Ocean and evolution of its continental margins. *Journal of Geophysical Research* **84**, 5973–6002.

Renne, P. R., Ernesto, M., Pacca, I. G., Coe, R. S., Glen, J. M., Prevot, M. & Perrin, M. (1992). The age of Paraná flood volcanism, rifting of Gondwanaland, and the Jurassic–Cretaceous boundary. *Science* **258**, 975–979.

Renne, P. R., Glen, J. M., Milner, S. C. & Duncan, A. R. (1996). Age of Etendeka flood volcanism and associated intrusions in southwestern Africa. *Geology* **24**, 659–662.

Renne, P. R., Marcia, E. & Milner, S. C. (1997). Geochronology of the Paraná–Etendeka Magmatic Province. *EOS Transactions, American Geophysical Union* **78**, F742.

Rollinson, H. (1993). *Using Geochemical Data.* Harlow, UK: Longman.

Schumacher, J. C. (1997). The estimation of ferric iron in electron microprobe analysis of amphiboles. *Mineralogical Magazine* **61**, 312–321.

Seth, B., Kroener, A., Mezger, K., Nemchin, A. A., Pidgeon, R. T. & Okrusch, M. (1998). Archaean to Neoproterozoic magmatic events in the Kaoko Belt of NW Namibia and their geodynamic significance. *Precambrian Research* **92**, 341–363.

Siedner, G. (1968). Structure and evolution of the Paresis igneous complex, South West Africa. *Transactions of the Geological Society of South Africa* **68**, 177–202.

Skjerlie, K. P. & Johnston, A. D. (1993). Fluid-absent melting behaviour of an F-rich tonalitic gneiss at mid-crustal pressures: implications for the generation of anorogenic granites. *Journal of Petrology* **34**, 785–815.

Steiger, R. H. & Jäger, E. (1977). Subcommission on geochronology; the use of decay constants in geo- and cosmochronology. *Earth and Planetary Science Letters* **36**, 359–362.

Stewart, K., Turner, S., Kelley, S., Hawkesworth, C. J., Kirstein, L. & Mantovani, M. (1996). 3-D, ^{40}Ar–^{39}Ar geochronology in the Paraná continental flood basalt province. *Earth and Planetary Science Letters* **143**, 95–109.

Streck, M. J. & Grunder, A. L. (1997). Compositional gradients and gaps in high-silica rhyolites of the Rattlesnake Tuff, Oregon. *Journal of Petrology* **38**, 133–163.

Tronnes, R. G. & Brandon, A. D. (1992). Mildly peraluminous high-silica granites in a continental rift; the Drammen and Finnemarka batholiths, Oslo Rift, Norway. *Contributions to Mineralogy and Petrology* **109**, 275–294.

Trumbull, R. B., Gerstenberger, H., Schmitt, A. K., Mingram, B., Bühn, B. & Emmermann, R. (1997). Mesozoic igneous complexes in Namibia: crust–mantle interaction on a rifted continental margin. *Terra Nova* **9**, *Abstract Supplement 1*, 459.

Turner, S. P., Foden, J. D. & Morrison, R. S. (1992). Derivation of some A-type magmas by fractionation of basaltic magma: an example from the Padthaway ridge, South Australia. *Lithos* **28**, 151–179.

Vervoort, J. D. & Patchett, P. J. (1996). Behaviour of hafnium and neodymium isotopes in the crust: constraints from Precambrian crustally derived granites. *Geochimica et Cosmochimica Acta* **60**, 3717–3733.

Watkins, R. T., McDougall, I. & le Roex, A. P. (1994). K–Ar ages of the Brandberg and Okenyenya igneous complexes, north-western Namibia. *Geologische Rundschau* **83**, 348–356.

Watson, E. B. (1979). Zircon saturation in felsic liquid: experimental results and application to trace elements geochemistry. *Contributions to Mineralogy and Petrology* **70**, 407–419.

Watson, E. B. & Harrison, T. M. (1983). Zircon saturation revisited: temperature and composition effects in a variety of crustal magma types. *Earth and Planetary Science Letters* **64**, 295–304.

Whalen, J. B., Currie, K. L. & Chappell, B. W. (1987). A-type granites: geochemical characteristics, discrimination and petrogenesis. *Contributions to Mineralogy and Petrology* **95**, 407–419.

Winkler, H. C. F. (1979). *Petrogenesis of Metamorphic Rocks*, 5th edn. Berlin: Springer.